Article

Structure-based design of 6-chloro-4-aminoquinazoline-2-carboxamide derivatives as potent and selective p21-activated kinase 4 (PAK4) inhibitors

Chenzhou Hao, Fan Zhao, Hong Yan SONG, Jing Guo, Xiaodong Li, Xiaolin Jiang, Ran Huan, Shuai Song, Qiaoling Zhang, Ruifeng Wang, Kai Wang, Yu Pang, Tongchao Liu, Tianqi Lu, Wanxu Huang, Jian Wang, Bin Lin, Zhonggui He, Haitao Li, Feng Li, Dongmei Zhao, and Maosheng Cheng

J. Med. Chem., **Just Accepted Manuscript** • DOI: 10.1021/acs.jmedchem.7b01342 • Publication Date (Web): 30 Nov 2017

	He, Zhonggui; Shenyang Pharmaceutical University, School of Pharmacy Li, Haitao; Tsinghua University, Tsinghua-Peking Joint Center for Life Sciences, Beijing Advanced Innovation Center for Structural Biology, Department of Basic Medical Sciences, School of Medicine Li, Feng; China Medical University, Department of Cell Biology, Key Laboratory of Cell Biology, Ministry of Public Health, and Key Laboratory of Medical Cell Biology, Ministry of Education Zhao, Dongmei; Shenyang Pharmaceutical University, Key Laboratory of Structure-Based Drug Design & Discovery of Ministry of Education Cheng, Maosheng; Shenyang Pharmaceutical University, Key Laboratory of Structure-Based Drug Design & Discovery of Ministry of Education

Structure-based design of 6-chloro-4-aminoquinazoline-2-carboxamide derivatives as potent and selective p21-activated kinase 4 (PAK4) inhibitors

Chenzhou Hao[†,§], Fan Zhao[∥,§], Hongyan Song[⊥,§], Jing Guo[†], Xiaodong Li[‡], Xiaolin Jiang[†], Ran Huan[‡], Shuai Song[†], Qiaoling Zhang[†], Ruifeng Wang[†], Kai Wang[†], Yu Pang[†], Tongchao Liu[†], Tianqi Lu[‡], Wanxu Huang[†], Jian Wang[†], Bin Lin[†], Zhonggui He[#], Haitao Li[∥], Feng Li*[‡], Dongmei Zhao*[†], Maosheng Cheng*[†]*

[†]Key Laboratory of Structure-Based Drug Design & Discovery of Ministry of Education, Shenyang Pharmaceutical University, Shenyang 110016, China

[‡]Department of Cell Biology, Key Laboratory of Cell Biology, Ministry of Public Health, and Key Laboratory of Medical Cell Biology, Ministry of Education, China Medical University, Shenyang 110001, China

[∥]Tsinghua-Peking Joint Center for Life Sciences, Beijing Advanced Innovation Center for Structural Biology, Department of Basic Medical Sciences, School of Medicine, Tsinghua University, Beijing 100084, China

[⊥]Institute of Materials Research and Engineering, A*STAR (Agency for Science, Technology and Research), 2 Fusionopolis Way, Innovis, #08-03, Singapore 138634

[#]School of Pharmacy, Shenyang Pharmaceutical University, Shenyang 110016, China

ABSTRACT

Herein, we report the discovery and characterization of a novel class of PAK4 inhibitors with a quinazoline scaffold. Based on the shape and chemical composition of the ATP-binding pocket of PAKs, we chose a 2, 4-diaminoquinazoline series of inhibitors as a starting point. Guided by X-ray crystallography and a structure-based drug design (SBDD) approach, a series of novel 4-aminoquinazoline-2-carboxamide PAK4 inhibitors were designed and synthesized. The inhibitors' selectivity, therapeutic potency, and pharmaceutical properties were optimized. One of the best compounds, **31** (CZh226), showed remarkable PAK4 selectivity (346-fold vs PAK1) and favorable kinase selectivity profile. Moreover, this compound potently inhibited the migration and invasion of A549 tumor cells by regulating the PAK4-directed downstream signaling pathways in *vitro*. Taken together, these data support the further development of **31** as a lead compound for PAK4-targeted anticancer drug discovery and as a valuable research probe for the further biological investigation of group II PAKs.

INTRODUCTION

The p21-activated kinases (PAKs) are serine/threonine (Ser/Thr) protein kinases that have been identified as downstream signaling effectors of Rho-family GTPases.[1, 2] The six mammalian PAK isoforms are categorized into two groups: PAK1-3 (group I) and PAK4-6 (group II), based on their structural homologies and biochemical

features.[3] As key components of the Ras-Rac/Cdc42-PAK pathway, PAKs have pivotal roles in many fundamental cellular processes, including cytoskeletal reorganization, focal adhesion, cell motility, morphological changes, cell-cycle progression, *etc*.[2] Moreover, the overexpression, amplification and mutational activation of PAK isoforms, in particular, PAK1 and PAK4, have been linked to many human diseases, including breast cancer, lung cancer, prostate cancer, colon cancer, and human head and neck squamous cell carcinoma.[4] Consequently, PAKs have emerged as attractive targets for new anticancer therapies and have been the subject of extensive drug discovery efforts.[5]

Although the two groups of PAK proteins are similar in overall sequence and structure, they are differentiated by their tissue expression profiles,[6] subcellular localization,[7] GTPase specificity,[7] activation mechanism,[8] and downstream substrate specificity.[2, 7] Studies using knockout mice lacking one or more specific PAK isoforms revealed the role of each isoform in normal tissue development, with phenotypes that range from no apparent effect to early embryonic death.[2, 9, 10] Among all of the PAKs, PAK4 is the most studied group II PAK member, and it has a place at critical nodal points in multiple signaling pathways that are associated with cell growth, cytoskeletal dynamics, cell polarity, survival, and development.[11] PAK4 is particularly highly expressed in prostate, testis, lung, heart, brain and liver.[12] It has attracted considerable interest because of its role in cancer invasion, metastasis and proliferation of BRAF- or KRAS-driven cancers.[13] In addition to PAK4, there is emerging evidence for the roles for PAK5 and PAK6 in cancer progression.[14]

Moreover, a recent study revealed that PAK2 inhibition correlates with increased acute cardiovascular toxicity, which may be enhanced by PAK1 inhibition.[15] Thus, the development of specific and potent PAK4 inhibitors is highly desirable for minimizing the risk of the potential side effects associated with the inhibition of normal function of group I PAKs and will also shed further light on its role in cancer progression.

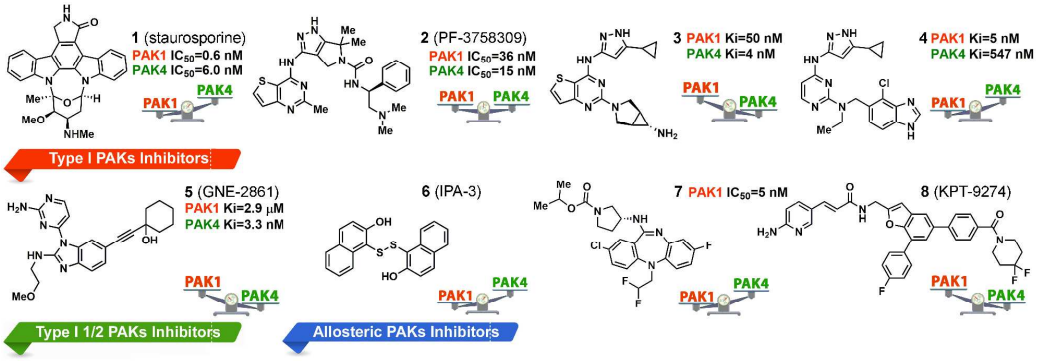

Figure 1. Classification of representative PAK inhibitors by mechanism of function.[5, 6]

Over the past two decades, several PAK inhibitors have been developed that exhibit different levels of selectivity across the PAK isoforms.[5, 6] On the basis of their binding modes, PAK inhibitors can be categorized into several types (Figure 1).[16] PF-3758309 (**2**),[17] a "Pan-PAK inhibitor", was the first compound advanced to phase I trials (NCT00932126) by Pfizer, targeting both group I and II PAKs. However, further development of **2** was called to a stop because of unsatisfactory pharmacokinetic data in phase I testing.[18] Compound **4**[19] and **5** (GNE-2861)[20] , a type I 1/2 kinase inhibitor, show significant group I and group II PAK selectivity, respectively. Most recently, a new dual PAK4/NAMPT modulator **8** (KPT-9274)[21] advanced to phase I human

clinical trials (NCT02702492) for the treatment of solid malignancies or non-Hodgkin's Lymphoma (NHL).

Our research group has focused on the discovery and optimization of PAK4 inhibitors as new therapeutic agents for over a decade,[22-24] and we identified quinazoline-based compound **9** (LCH-7749944) as a moderate PAK4 inhibitor *via* structure-based virtual screening in 2012.[22] Compound **9** was notable in that it possessed higher potency against PAK4 than PAK1 and significantly inhibited the migration and invasion of human gastric cancer cells in conjunction with the concomitant blockage of the PAK4/LIMK1/cofilin and PAK4/MEK-1/ERK1/2/MMP2 pathways. Herein, we describe our structure-based design efforts toward the discovery of potent group II PAK inhibitors specifically targeting PAK4 and the structure-activity relationship for this series. Our goal for optimization was to improve the group II inhibitory activity of early lead **10a** while maintaining high selectivity over group I PAKs (PAK1 and PAK4 as representatives for group I and group II PAKs, respectively). The binding mode revealed in the X-ray crystallographic studies of **10a**, combined with analysis of the residue differences among PAK isoforms, shed light on some of the selectivity determinants within the ATP binding site. The following optimization led to the discovery of compound **31**, a potent PAK4 inhibitor with substantially lower inhibition for group I PAKs (Figure 2).

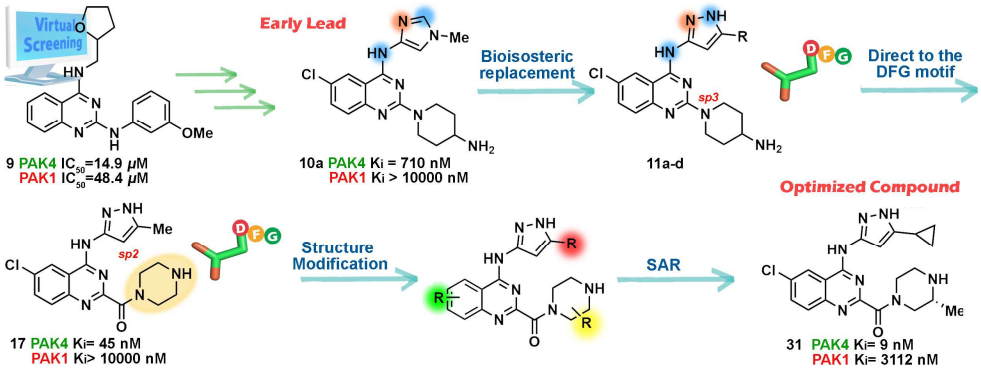

Figure 2. The design and modification strategies of novel and selective PAK4 inhibitors.

RESULTS AND DISCUSSION

Identification and Characterization of Early Lead 10a. Inspired by our previous study of the PAK4 inhibitor **9**,[22] we identified compound **10a** as a moderately potent biochemical inhibitor of PAK4 (PAK4 K_i = 0.710 μM) without measurable binding to PAK1 (PAK1 K_i > 10 μM) from a collection of quinazoline derivatives. For an independent confirmation of activity and to address potential secondary effects in the biochemical assay, such as PAK4 conformation change induced by peptide substrate effect, or fluorescent false signal, two direct binding assays were used to identify the binding between **10a** and the truncated PAK4. Differential scanning fluorimetry (DSF)[25] showed a melting temperature shift of 0.5 °C for the compound **10a**-PAK4 complex compared to the truncated PAK4 protein (Supporting Information Table S4). Surface plasmon resonance (SPR)[26] assay resolved the dissociation constant of **10a** with PAK4 to be 0.156 μM, by multi-concentration kinetic analysis and fitted by 1:1 binding mode. The results demonstrate that compound **10a** binds directly to the truncated PAK4 kinase domain.

To gain insight into the origin of the PAK4 selectivity (PAK1 K_i/PAK4 K_i) displayed by compound **10a** (> 14-fold), the crystal structure of PAK4 kinase domain in complex with compound **10a** was obtained. The co-crystal structure determined at 2.65 Å resolution (Supporting Information Table S1) clearly shows that PAK4 adopts an active conformation (DFG-in) with a salt bridge (2.3 Å) between Lys350 and Glu366 in helix αC, and **10a** is located in the ATP binding cleft between the N- and C-lobes (Figure 3). The imidazole ring of **10a** aligns in the hinge region, forming two H-bonds with the main chain of Leu398, and an additional non-classical H-bond (3.0 Å) is formed between Glu396 and the C2-H of the amino imidazole.[27] The N-1 methyl group makes effective hydrophobic interactions with Met395, the gatekeeper residue. A favorable electrostatic quinazoline N3 to imidazole C5 interaction was proposed to orient these rings in a coplanar manner. The piperidine NH_2 group makes a hydrogen bond to the backbone carbonyl of Glu329 (glycine rich loop/P-loop) of 2.9 Å. The co-crystal structure confirmed that **10a** is a typical type I inhibitor that binds to the hinge region without perturbing the DFG-in state. The simplicity of the molecule (MW = 357.5) and its reasonable binding efficiency[28] (LE = 0.31) made it an attractive starting point for further optimization.

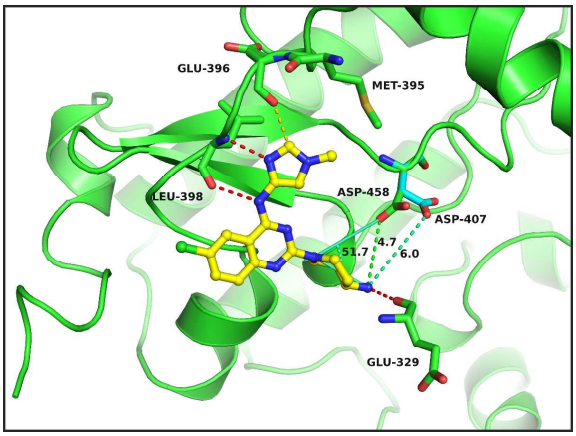

Figure 3. The crystal structure of PAK4 in complex with **10a** (PDB code 5XVF). Note: Asp458 is oriented towards the NH_2 in the piperidine of **10a** compared to its counterpart Asp407 in PAK1 as in the structure 4O0R (cyan stick). The distance between the piperidine NH_2 of **10a** and the carboxyl group (OD2 atom) of $Asp458^{PAK4}$ and $Asp407^{PAK1}$ is 4.7 Å and 6.0 Å, respectively (green line). The ∠ $O_{(Asp458)}$–$N_{(piperidine\ N)}$–$N_{(piperidine\ NH_2)}$ angle is approximately 51.7° (cyan line).

To further improve the binding affinity of compound **10a**, SAR at the hinge binding motif was explored based on the structural insight provided by the crystal structure above. As shown in Table 1, the role of the N-1 group in imidazole analogues is critical, as cyclopropyl analog **10b** and isopropyl analog **10c** exhibited similar inhibitory activity with methyl **10a**, while the activity of bulky phenyl **10d** was only half of **10a**. Pyrazole analogues **11a** [PAK4 K_i = 0.099 μM, PAK4 K_d (SPR) = 0.043 μM] and **11b** [PAK4 K_i = 0.016 μM, PAK4 K_d (SPR) = 0.006 μM] were found to exhibit significantly improved biochemical and cellular potency (data not shown) when the donor C-H hydrogen bond to the hinge in **10a** is replaced by a N-H in **11**. Such results clearly showed that the non-classical C-H hydrogen bond is not as good

as the classical N-H hydrogen bond in this case and the change of the hydrogen bond from the non-classical type to the classical type led to significant improvement. The 1*H*-pyrazol-3-amine as the hinge binding motif was maintained in the following optimization. Although the pyrazole analogues showed dramatically improved inhibitory activities against PAK4, they unfortunately did not lead to any improvement in their PAK4/1 selectivity relative to **10a** (**11a**, 18-fold; **11b**, 19-fold). To discover PAK4 inhibitors with better selectivity over PAK1, next we sought to exploit the subtle differences between PAK4 and PAK1 crystallographic data available in the PDB database.

Table 1. SAR of the initial optimization of the hinge binding motif.

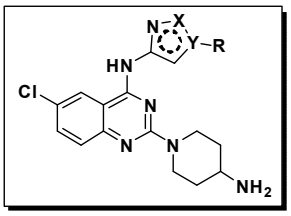

Compound	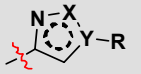	PAK4 K_i[a] (μM)	PAK1 K_i[a] (μM)	PAK4[b] select.index	clogP[c]	PSA[d]	LE[e]/LLE[f]
10a	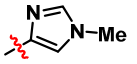	0.710	>10	>14x	2.6	71.3	0.34/3.61
10b	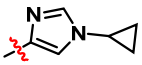	0.652	ND[g]	ND	3.0	70.9	0.32/3.19
10c	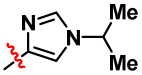	0.884	ND	ND	3.2	70.4	0.31/2.85
10d	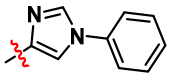	1.440	ND	ND	3.8	71.0	0.27/2.04
11a	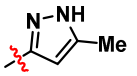	0.099	1.891	19x	2.3	86.4	0.39/4.67
11b	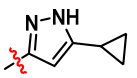	0.016	0.288	18x	2.9	85.0	0.40/4.85
11c	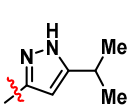	0.077	ND	ND	3.1	84.8	0.37/4.01

11d	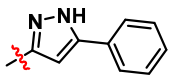	0.256	ND	ND	3.5	85.1	0.31/3.09
1	-	0.009/ (0.006)[h]	0.003/ (0.0006)[h]	0.3x/ (0.1x)[h]	3.7	69.8	0.32/4.35
2	-	0.026/ (0.015)[i]	0.052/ (0.036)[i]	2.0x/ (2.4x)[i]	4.3	98.3	0.30/3.29

[a]PAK4 and PAK1 kinase inhibition was determined using a FRET-based Z'-Lyte assay according to the manufacturer's instructions (Invitrogen, Carlsbad, USA). The K_i values are the average of at least two duplicate experiments. SEM < ±20 %. [b]PAK1 K_i/ PAK4 K_i, x = fold. [c]The clogP values were calculated by the Qikprop software with default settings (pH = 7.0). [d]Van der Waals surface area of polar nitrogen and oxygen atoms. Calculated by the Qikprop software. [e]Ligand efficiency = (-1.4 log K_i)/(n heavy atoms).[28] [f]Ligand-lipophilicity efficiency = (-log K_i) - (cLogP).[29] [g]ND = not determined. [h]Reported data.[19] [i]Reported data.[19]

Active-site Sequences and Structures of Group I and II PAKs: Rational Design of a New Series of PAK4 Inhibitors by Targeting the DFG Motif. Like all other typical protein kinases, the kinase domain of PAKs consists of a N-terminal domain and a C-terminal domain that are connected *via* a hinge.[30] As shown in Figure 4A, the ATP binding pocket is located between the two lobes. The selective inhibition of PAK4 over group I PAKs has proven to be a challenging endeavor, in part because of the high sequence homology within the ATP binding site of the PAKs (Supporting Information, Figure S1). To address this challenge, we exploited the three-dimensional structures of PAKs and defined the ATP binding pocket as a set of 40 residues (P1 through P40, starting at the N-terminus, in Figure 4A) able to interact with ATP-competitive inhibitors (checked using KLIFS, a structural kinase-ligand

interaction database).[31, 32] The direct comparison of the residues set at the primary sequence level revealed that more than 65 % (26/40) of residues are conserved in the respective ATP pockets of PAK1 and PAK4 (Figure 4C). We believe that sequence variations and unique active site features among PAKs will provide opportunities for the selective targeting of these family members.[16]

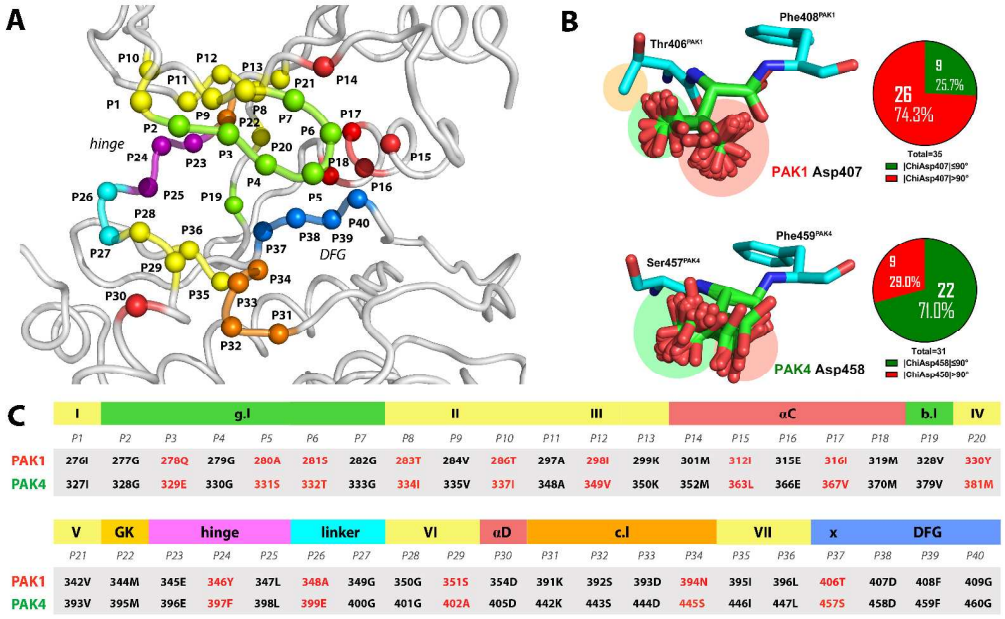

	I	g.l						II			III			αC					b.l	IV
	P1	P2	P3	P4	P5	P6	P7	P8	P9	P10	P11	P12	P13	P14	P15	P16	P17	P18	P19	P20
PAK1	276I	277G	278Q	279G	280A	281S	282G	283T	284V	286T	297A	298I	299K	301M	312I	315E	316I	319M	328V	330Y
PAK4	327I	328G	329E	330G	331S	332T	333G	334I	335V	337I	348A	349V	350K	352M	363L	366E	367V	370M	379V	381M

	V	GK	hinge			linker		VI		αD	c.l				VII		x	DFG		
	P21	P22	P23	P24	P25	P26	P27	P28	P29	P30	P31	P32	P33	P34	P35	P36	P37	P38	P39	P40
PAK1	342V	344M	345E	346Y	347L	348A	349G	350G	351S	354D	391K	392S	393D	394N	395I	396L	406T	407D	408F	409G
PAK4	393V	395M	396E	397F	398L	399E	400G	401G	402A	405D	442K	443S	444D	445S	446I	447L	457S	458D	459F	460G

Figure 4. A comparison of the ATP-binding pocket between group I and II PAKs. (A) The structure of the PAK kinase domain (generated from the PDB structure 2X4Z). Residues contributing to the binding cleft (P1-P40) are depicted as spheres. (B) Alignment (main chain atoms only) of the DFG-aspartate of PAK1 and PAK4 in the active state. An updated survey of all PDB PAK1 structures in the active DFG-in state indicated that 74 % (26/35) of the DFG-aspartate side chain is pointing away from the ATP-competitive ligand. For the corresponding residue in PAK4, 71 % (22/31) of the DFG-aspartate side chain is pointing toward the ligand. Figures were generated using PyMOL (The PyMOL Molecular Graphics System, Version 1.7.2 Schrödinger,

LLC.). The definition of the dihedral angles χ1(chi): N-Cα-Cβ-Cγ. (C) Sequence alignment of the residues surrounding the ATP binding site in PAK1 and PAK4. Differential residues between the two kinases are highlighted.

Most protein kinases share a strictly conserved DFG (Asp-Phe-Gly, P38-P40) motif in the ATP site that can adopt two distinct conformations, the active DFG-in and the inactive DFG-out states.[16] Further alignment of the protein crystal structures available in the Protein Data Bank (PDB) revealed that the orientation of the PAK4 DFG-aspartate ($Asp458^{PAK4}$) side chain is different from the corresponding residue in PAK1 ($Asp407^{PAK1}$).[19] As a proof of concept, Crawford et *al.* proved that taking advantage of differing orientations of the DFG Asp motif serves as a viable means to design Group I selective PAK inhibitors.[19] An updated survey of all PDB PAK1 structures in the active DFG-in state indicated that 74 % (26/35) of the DFG-aspartate side chain is pointing away from the ATP-competitive ligand, and for the corresponding residue in PAK4, 71 % (22/31) of the DFG-aspartate side chain is pointing toward the ligand (Figure 4B, see the Supporting Information for details). Presumably, this can be explained by a key residue difference in the DFG-1 residue (P36, Thr^{406} in PAK1 and Ser^{457} in PAK4): there is potentially an unfavorable interaction of the larger, branched Thr residue with the Asp residue in PAK1. In the active DFG-in conformation, the aspartate is required to chelate Mg^{2+} and helps to orient the γ-phosphate for its transfer.[33] The important biological function of the DFG motif and orientation differences in the DFG Asp ($Asp458^{PAK4}$/$Asp407^{PAK1}$)

suggested to us that the modification of the early lead compounds by specifically targeting the DFG motif would enhance PAK4 inhibitory activity and selectivity.

Indeed, the PAK4/**10a** crystal structure showed that the distance from piperidine NH_2 to the side chain of Asp458 is 4.7 Å, and the $\angle O_{(Asp458)}-N_{(piperidine\ N)}-N_{(piperidine\ NH2)}$ angle is 51.7° (Figure 3), which could allow the installation of an appropriate moiety to interact with the DFG motif. Furthermore, to generate electrostatic interactions or hydrogen binding with the negatively charged residue $Asp458^{PAK4}$ through the quinazoline C2 position, the side chain should adopt an appropriate angle to ensure that it could make favorable interactions with the DFG motif. In light of this, we incorporated a putative DFG binding moiety to the central core of **10a** by tethering a cationic amino group or hydrogen bond donor (HBD) group through an amide carbonyl linkage in consideration of its *sp2* hybridization. In doing so, a novel 4-((1*H*-pyrazol-3-yl)-amino)quinazoline-2-carboxamide scaffold was designed by inserting a carbonyl group at the C2 side chain of our initial set of compounds (see Table 2).

Structural Modification and SAR Interpretation. The inhibitory activities of the designed compounds for PAK1 and PAK4 were first evaluated *via* a well-established fluorescence resonance energy transfer (FRET)-based Z'-Lyte assays (Invitrogen, Carlsbad, USA). Two well characterized PAK inhibitors, **1**[34] and **2**[17], were used as positive controls.

Following the rational design approach above, the incorporation of various tail amide group led to compounds **12-17** with diverse activities (Table 2). The

4-amino-piperidines **12** and **14** displayed a decrease in PAK4 affinity compared to **11a**, with K_i values of 0.354 and 0.674 μM, respectively. Meanwhile, alcohol analogues **13** and **15** lost an order of magnitude in potency, suggesting that the amino group at the tail position is preferable presumably to interact with the side chain of $Asp458^{PAK4}$ *via* forming a hydrogen bond or ionic interactions. The methylation of the NH_2 as in **16** resulted in a decrease by half. The overall trend of decreasing activity is probably due to steric hindrance with the introduction of a slightly bulkier functional group at the terminal position of the piperidine ring and more importantly, the introduction of the carbonyl group between the quinazoline moiety and the piperidine moiety (Supporting Information, Figure S2C and S2D). Such evidence prompted us to try to contract the exo nitrogen atom into an endo one, which led to compound **17**. As expected, compound **17** showed dramatically improved binding affinities [PAK4 K_i = 0.045 μM, PAK4 K_d (SPR) = 0.066 μM] over those of **12**. Compared to the 2, 4-diaminoquinazoline analogue **11a**, the introduction of an amide sidechain in compound **17** was clearly essential in improving its PAK4 selectivity (18 fold vs > 222-fold, as shown in Table 3). A molecular docking simulation predicted that the two compounds adopted very similar conformations, and their aromatic rings superimposed very well. The most significant difference between these two inhibitors is the additional interactions between the piperazine moiety and the DFG binding motif of PAK4, which likely provided a charge-assisted hydrogen bond[35] (CAHB, traditional hydrogen bonding is accompanied by Coulombic interactions) interactions with the deprotonated carboxylic acid side chain of $Asp458^{PAK4}$ (2.3 Å, Figure 5A).

To obtain more insight into the interactions critical to the excellent activity of compound **17**, compounds **18-20** were designed, synthesized and evaluated. Unsurprisingly, the importance of this electrostatic interaction is elucidated by the fact that compound **18** [PAK4 K_i = 2.172 μM, PAK4 K_d (SPR) = 1.940 μM], in which the positively charged nitrogen atom was replaced with an oxygen atom, is a very poor inhibitor (Figure S2E and S2F). Compound **19,** an *N*-methylated derivative of **17**, was 17-fold less active, highlighting the importance of the amine proton acting as a hydrogen bond donor. When the amine proton was replaced by an amide proton (**20**, PAK4 K_i = 2.408 μM), the activity was decreased by 54-fold (Figure S2G and S2H). The dramatic decrease in activity could be attributed to the fact that the amide group could not form salt bridge interactions with the side chain of $Asp458^{PAK4}$. Furthermore, changing the piperazine ring to other heterocyclic secondary amines was not tolerable, as indicated by the activities of compounds **21-24**. This indicated that the conformation of the amide side chain is critical to the activity of the compounds. The cyclopropyl analog **25** [PAK4 K_i = 0.016 μM, PAK4 K_d (SPR) = 0.016 μM, PAK1 K_i = 2.750 μM] showed improved activity, but its selectivity was not improved (172-fold, shown in Table 3). In summary, an additional hydrogen bond conjoins with strong salt bridge interactions, and the correct orientation of the piperazine ring likely explains the enhanced activity and selectivity of **17** and **25**.

Table 2. The SAR of carboxamide substituents.

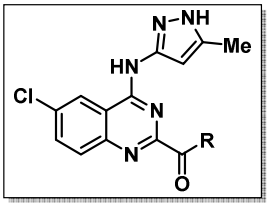

Compound	R	PAK4 K_i[a] (μM)	Compound	R	PAK4 K_i[a] (μM)	Compound	R	PAK4 K_i[a] (μM)
12	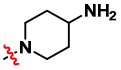	0.354	**17**		0.045	**22**	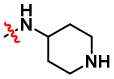	0.325
13	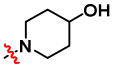	3.817	**18**		2.172	**23**[b]		1.630
14	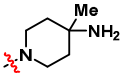	0.674	**19**	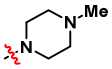	0.768	**24**	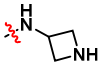	0.782
15	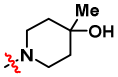	3.890	**20**	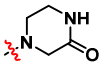	2.408	**1**	-	0.009
16	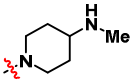	0.672	**21**	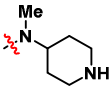	0.576	**2**	-	0.026

[a]PAK4 kinase inhibition was determined using a FRET-based Z'-Lyte assay according to the manufacturer's instructions (Invitrogen, Carlsbad, USA). The K_i values are the average of at least two duplicate experiments. SEM <±20 %. [b]Racemic mixture.

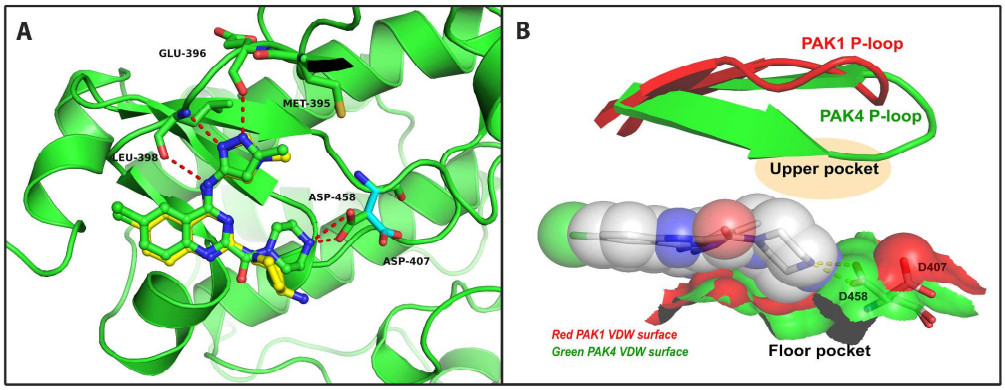

Figure 5. The predicted binding mode of **17**. (A) The superimposition of structures of **17** (green) with **10a** from the crystal structure (PDB code 5XVF). PDB entry 2X4Z was used for molecular docking simulation with Autodock4. Note: Asp458 in PAK4

overlaid with a key residue different in PAK1 (cyan, Asp407 from structure 4O0R). (B) The overlay of PAK4 and PAK1 with **17** (generated from the PDB structures 2X4Z and 4O0R, respectively).

Beginning with the new scaffold of compounds **17** and **25**, further structural optimization was undertaken to enhance the binding affinity of the inhibitors by increasing the spatial occupancy of the kinase ATP pocket. Meanwhile, the "floor pocket" on the bottom of the ATP binding pocket near the DFG motif and the "upper pocket" beneath the glycine rich loop (P-loop) also captured our attention (shown in Figure 5B). In contrast, PAK1 has a much wider and shallower "floor pocket", and PAK4 has a deeper and overall smaller sub-pocket. This difference in size was attributed to the distinct conformations of DFG Asp, as mentioned above, and key residues differences inside the sub-pocket ($Ser457^{PAK4}$ vs $Thr406^{PAK1}$; $Ser445^{PAK4}$ vs $Asn394^{PAK1}$). Because of the subtle conformation differences in the P-loop (shown in Figure 5B), the specific features of the "upper pocket" in different PAK isoforms were also observed. It was apparent from the modeling structures that these hydrophobic pockets are located around the piperazine ring of **17** and could be accessed *via* an axial substituent on the piperazine ring. We hypothesized that an improvement in the binding affinity and selectivity might be achieved by targeting these sub-pockets. Table 3 shows our efforts at potency optimization through piperazine substitution. The analogues with the methyl group positioned next to the amide nitrogen (compounds **26-29**) were proven unsuccessful at improving potency and selectivity. Among them, the compounds with a (*R*)-configuration at the methyl

stereocenter (**28, 29**) exhibited better potency and selectivity than their corresponding (*S*)-analogues (**26, 27**). A significant improvement in PAK4 selectivity was obtained by incorporating a (*R*)-methyl group next to the amine nitrogen on the piperazine ring (**30, 31**), which most likely contributes to their shape complementarity to maximize van der Waals contacts. In the end, compound **31** had robust PAK4 affinity (PAK4 K_i = 0.009 μM) and excellent selectivity at 346-fold over PAK1 (PAK1 K_i = 3.112 μM), comparable to that of **5** (PAK1 K_i = 2.9 μM[20]). Interestingly, the (*S*)-methyl substituent (**32, 33**) was not tolerated, suggesting that chirality is a crucial element that influences van der Waals interactions. The bulky (*R*)-ethyl analogue, **36** (PAK4 K_i = 0.006 μM, PAK1 K_i = 0.368 μM), displayed similar potency against PAK4 in the single digital nanomolar range, but it had little selectivity against PAK4 (61-fold). Further substitution of the piperazine ring, however, resulted in a significant decrease in activity (dimethyl analogues **34** and **35**).

Table 3. The *in vitro* biological and physical properties of piperazine analogues.

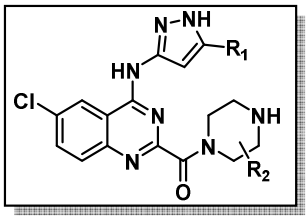

Compound	R_1	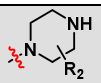	PAK4 K_i[a] (μM)	PAK1 K_i[a] (μM)	PAK4 select.index[b]	clogP[c]	p*Ka*[d]	PSA[e]	LE[f] /LLE[g]
17	Me		0.045	>10	>212x	1.6	7.8	98.7	0.40/5.78
25	*c*-Pr		0.016	2.750	172x	2.2	7.8	97.4	0.39/5.63
26	Me		0.218	>4.52	>21x	2.4	8.0	91.4	0.35/4.30
27	*c*-Pr		0.026	0.383	15x	3.0	8.0	90.1	0.37/4.61
28	Me		0.151	>4.52	>30x	1.9	8.0	92.5	0.35/4.94

29	*c*-Pr		0.017	2.080	122x	2.5	8.0	91.1	0.38/5.29
30	Me	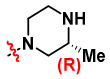	0.051	>10	>196x	2.0	7.9	97.5	0.38/5.34
31	*c*-Pr		0.009	3.112	346x	2.6	7.9	96.2	0.39/5.49
32	Me		0.306	>4.52	>15x	2.0	7.9	97.5	0.34/4.57
33	*c*-Pr		0.028	0.690	25x	2.6	7.9	96.1	0.36/4.99
34[i]	Me	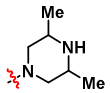	0.119	ND[h]	ND	2.2	8.0	95.5	0.35/4.72
35[i]	*c*-Pr		0.114	>4.52	>40x	2.8	8.0	94.1	0.32/4.11
36	c-Pr	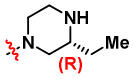	0.006	0.368	61x	2.9	8.0	94.0	0.38/5.29
1	-	-	0.009	0.003	0.3x	3.7	9.6	69.8	0.34/4.82
2	-	-	0.026	0.052	2.0x	4.3	8.1	98.3	0.30/3.30

[a]PAK4 and PAK1 kinase inhibition was determined using a FRET-based Z'-Lyte assay according to the manufacturer's instructions (Invitrogen, Carlsbad, USA). The K_i values are the average of at least two duplicate experiments. SEM <±20 %. [b]PAK1 K_i/ PAK4 K_i, x = fold. [c]The clogP values were calculated by the Qikprop software with default settings (pH = 7.0). [d]The p*K*a values were calculated using ChemAxon's MarvinSketch (version 5.4.11). [e]The van der Waals surface area of polar nitrogen and oxygen atoms. Calculated by the Qikprop software. [f]Ligand efficiency = (-1.4 log K_i)/(n heavy atoms).[28] [g]Ligand-lipophilicity efficiency = (-log K_i) - (cLogP).[29] [h]ND = not determined. [i]Mixture of diastereomers.

To better understand the origin of the excellent PAK4 selectivity, the crystal structures of the PAK4 kinase domain in complex with **31** (PDB code 5XVG) and its highly similar methyl analogue **30** (PDB code 5XVA) were solved to 2.10 and 1.85 Å, respectively (Supporting Information Table S1). The binding mode observed for **31** was consistent with that observed with **30** (Figure 6), and the key interactions are shown in Figure 7. The aminopyrazole of **31** forms classic donor-acceptor-donor

H-bond interactions with the hinge region (carbonyl of Glu396^{PAK4}; carbonyl and NH of Leu398^{PAK4}), which is similar to that observed in the crystal structure of PAK4 in complex with **10a**. The cyclopropyl moiety makes effective hydrophobic interactions with Met395^{PAK4}, the gatekeeper residue, and Val335^{PAK4}. Consistent with our hypothesis, the NH on the piperazine ring forms a charge-assisted hydrogen bond with the negatively charged residue Asp458^{PAK4} through the amide carbonyl linkage, with a distance of 2.8 Å. It is noteworthy that the carboxylic side chain of Asp444^{PAK4} induces conformational changes to form electrostatic interactions with the tail of **31** (3.4 Å). In comparison with the putative structure of PAK1/**31**, the side chain of Asp407^{PAK1} is pointing away from compound **31** and hence not able to form electrostatic interactions with the piperazine ring (Figure 7B). Additionally, the piperazine ring of **31** makes a lipophilic contact with the "floor pocket" of PAK4 mentioned above, and the (*R*)-methyl group of the piperazine ring fills a hydrophobic dimple in the glycine rich loop above, which also explains why an additional (*R*)-methyl group increased the binding affinity and selectivity for PAK4. The differences in the binding modes for **31** to PAK4 and PAK1 are also directly linked to the differences in docking scores (X-score[36]: −8.95 for PAK4 and −6.75 for PAK1) and to the experimentally observed selectivity. The beneficial van der Waals interactions resulting from shape complementarity as well as the anticipated CAHB with Asp458^{PAK4} contribute to the increased binding affinity of **31**, demonstrating the rationale of our optimization hypothesis, thereby providing a molecular explanation for the subtype selectivity.

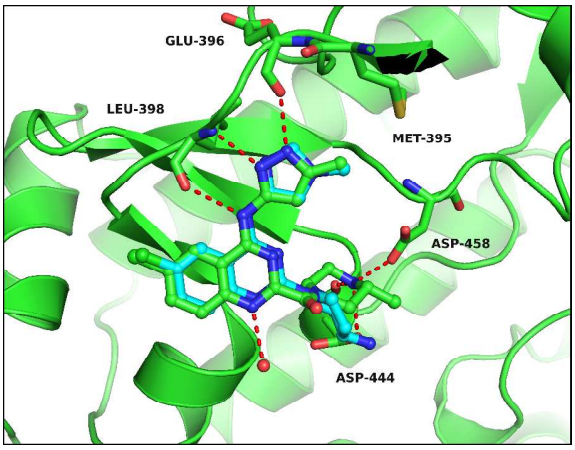

Figure 6. The crystal structure of PAK4 in complex with **30** (PDB code 5XVA). Superimposition of the structures of **30** (green) with **10a** (cyan) from the crystal structure (PDB code 5XVF).

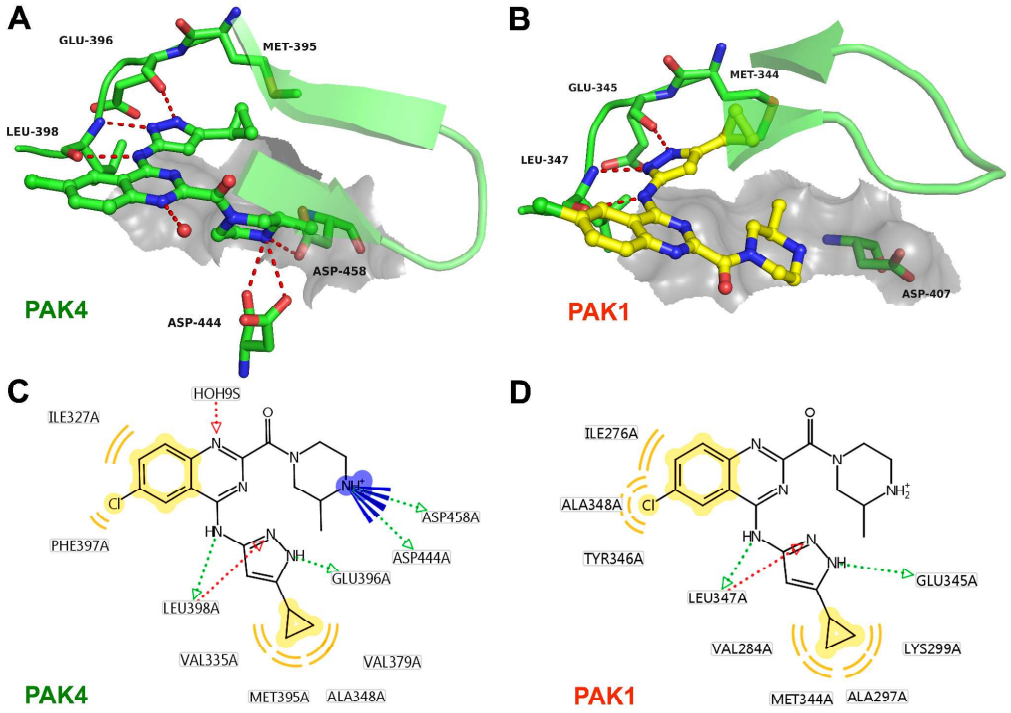

Figure 7. (A) The crystal structure of PAK4 in complex with **31** (PDB code 5XVG). (B) Predicted binding mode of **31** in PAK1 (PDB code 4O0R). A schematic representation of the contacts between **31** and the binding site residues of PAK4 (C)

and PAK1 (D) was visualized by LigandScout.[37] Note: the piperazine ring of **31** provides charge-assisted hydrogen bond (CAHB) interactions with Asp458^{PAK4} and Asp444^{PAK4}.

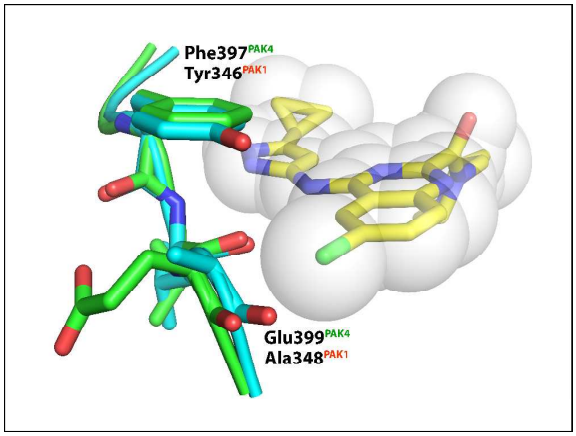

Figure 8. Microenvironment of the 6-substituent of the inhibitors. The X-ray structure of **31** in complex with PAK4 (green, PDB 5XVG) overlaid with key residue differences with PAK1 (cyan, Tyr346 and Ala348 from structure 4O0R).

Lastly, the role of the substituent at the C-6 position of the quinazoline core was investigated, and the data are summarized in Table 4. As shown in Figure 8, the 6-chloro group lies in the clifflike entrance around the hinge area and leads to van der Waals interactions with Phe397^{PAK4}, Glu399^{PAK4} and Ile327^{PAK4} (P24, P26, and P1 in Figure 4B, respectively). To probe this distinctive entrance region, the removal of the chloro group (compound **37,** PAK4 K_i = 0.017 μM) caused a slight decrease in the potency for PAK4 and a significant reduction in PAK4/1 selectivity (**37**, PAK4 selectivity: 63-fold). In addition, the position of the chloro group was also found to affect the selectivity profile. Although the 7-chloro derivative **38** (PAK4 K_i = 0.006 μM) displayed better potency than that of **31**, it suffered from reduced PAK4

selectivity (**38**, PAK4 selectivity: 57-fold). Further investigation suggested that the 6-chloro group in **31** could be replaced by electron-withdrawing substituents, such as F (**39**) and Br (**40**), and still retain its strong PAK4 affinity but the PAK4 selectivity was reduced by variable degrees (PAK4 selectivity: 31-fold and 190-fold, respectively). The compound bearing large electron-donating group, such as a methoxyl group (**41**), suffered from reduced potency for both PAK1 and PAK4 (PAK4 K_i = 0.036 μM; PAK1 K_i > 4.52 μM). These key findings highlighted that the importance of both shape and electrostatic complementarity at the 6-position of the quinazoline core because the residues around the 6-position between PAK4 and PAK1 are not conserved (Phe397^{PAK4} vs Tyr346^{PAK1}; Glu399^{PAK4} vs Ala348^{PAK1}, Figure 8). It may be possible to further exploit such sequence differences for the future design of inhibitors that distinguish PAK4 and PAK1 to a larger extent.

Table 4. The SAR of the quinazoline core.

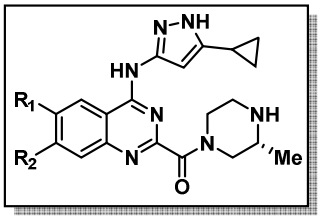

Compound	R_1	R_2	PAK4[a] Ki (μM)	PAK1[a] Ki (μM)	PAK4 select.index[b]	clogP[d]	p*Ka*[e]	PSA[f]	LE[g]/LLE[h]
31	Cl	H	0.009	3.112	346x	2.6	7.9	96.2	0.39/5.49
37	H	H	0.017	1.072	63x	2.1	7.9	95.6	0.39/5.69
38	H	Cl	0.007	0.401	57x	2.6	7.9	95.6	0.39/5.60
39	F	H	0.016	0.503	31x	2.3	7.9	96.2	0.38/5.48
40	Br	H	0.011	2.085	190x	2.6	7.9	95.6	0.38/5.34
41	OMe	H	0.036	>4.52	>126x	2.2	7.9	104.6	0.35/5.26

[a]PAK4 and PAK1 kinase inhibition was determined using a FRET-based Z'-Lyte assay according to the manufacturer's instructions (Invitrogen, Carlsbad, USA). The

K_i values are the average of at least two duplicate experiments. SEM <±20 %. [b]PAK1 K_i/ PAK4 K_i, x = fold. [c]Determined by differential scanning fluorimetry (DSF). [d]The clogP values were calculated using the Qikprop software with the default settings (pH = 7.0). [e]The p*K*a values were calculated using ChemAxon's MarvinSketch (version 5.4.11). [f]The van der Waals surface area of polar nitrogen and oxygen atoms. Calculated using the Qikprop software. [g]Ligand efficiency = (-1.4 log K_i)/(n heavy atoms).[28] [h]Ligand-lipophilicity efficiency = (-log K_i) - (cLogP).[29]

After several rounds of lead optimization aided by X-ray crystallography and molecular docking simulations, several compounds were identified with significant inhibitory potency against PAK4 with K_i values higher than or compatible to the reference compound **2**. Over the course of the optimization, a high degree of ligand efficiency was maintained, with LE ≥ 0.38 and LLE ≥ 5.3 for the majority of sub-20 nM K_i compounds. Among them, compound **31** demonstrated the best balance of potency, selectivity, and desirable physicochemical properties (p*K*a = 7.93, clogP = 2.54, PSA = 96.1). Encouraged by the potency of **31** and its selectivity over PAK1, its kinome selectivity profile was investigated by determining % inhibition at 0.1 μM and 1.0 μM (concentration equal to 11-fold and 110-fold above PAK4 K_i, respectively) against a panel of 54 kinases at the ATP K_m concentration, and the full data set is available in the supporting information. Good kinase selectivity was observed for **31**, with only PAK4 producing greater than 80 % inhibition at the screening concentration of 0.1 μM (PAK4 IC_{50} = 0.0111 μM, Figure 9). These data demonstrated that compound **31** is a potent PAK4 inhibitor with good kinase spectrum selectivity.

Although the DFG motif is highly conserved among protein kinases, the proper spatial arrangement of **31** with the DFG motif of PAK4 in combination with other residues differences within the ATP binding site would likely explains the selectivity of **31**.

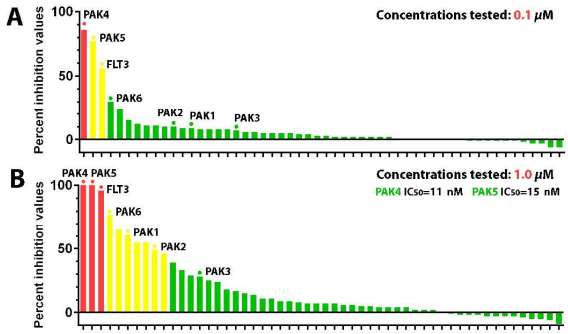

Figure 9. Selectivity profile of compound **31** (A) measured at a concentration of 0.1 μM and (B) 1.0 μM in a panel of 54 kinases generated with the SelectScreen® Profiling Service from Life Technologies (red columns denote >80 %, yellow columns between 40 and 80 %, and green columns <40 % inhibition).

Cellular effects of Compound 31. Previous studies have shown that PAK4 is overexpressed in several non-small cell lung cancer (NSCLC) cell lines and human NSCLC tissues.[12, 38] Increased expression of PAK4 was correlated with metastasis, shorter overall survival, advanced stage of NSCLC. Furthermore, selective suppression of PAK4 with siRNA has been shown to substantially suppress the migration and invasion of the PAK4-dependent A549 cells (human lung adenocarcinoma epithelial cell).[38] Considering the potent PAK4 inhibition of compound **31**, we first investigated its anti-proliferative effects on A549 cells. Meanwhile, the tumour cell line NCI-H460 (human large cell lung cancer cell), whose

growth was not dependent on PAK4, and HEK-293 cells (human embryonic kidney 293 cell) were used to test the potential off-target effects of potent PAK4 inhibitors. It was shown that compound **31** has moderate antiproliferative activities against A549 cells (Figure 10A), which is similar to the previous observation of **5** on MDA-MB-436 and MCF10A PIK3CA cells.[20] The relatively low cell growth inhibitory activities suggested that PAK4 might not be the "driving force" for proliferation of these cancer cells. Next, the effects of compound **31** on tumor cell migration and invasion were assessed using wound healing and transwell assays. Microphotographs showed that untreated A549 cells filled most of the wounded area 2 days after scratching the cell monolayer, whereas treatment with indicated doses of compound **31** significantly suppressed the wound healing (Figure 10B). Compound **31** treatment also significantly inhibited the A549 cells migration (Figure 10C, E) and invasion (Figure 10D, F) by transwell assay. In contrast, the decrease in cell migration and invasion was not pronounced in NCI-H460 and HEK-293 cells (Figure 10G-J), suggesting that inhibition of cell motility by compound **31** is in fact related to PAK4 inhibition. To further illustrate the mechanism, the effects of compound **31** on the PAK4/LIMK1/cofilin, PAK4/MMP2, or PAK4/GEF-H1 signaling pathways were examined by Western blot analysis. As shown in Figure 10K, phosphorylation of PAK4, LIMK1, and cofilin were inhibited by compound **31** treatment in dose-dependent manner. Furthermore, phosphorylation of Ser810 on GEF-H1 and expression of MMP-2 were also inhibited by compound **31**, which may contribute to its anti-metastasis effect of A549 lung cancer cells.

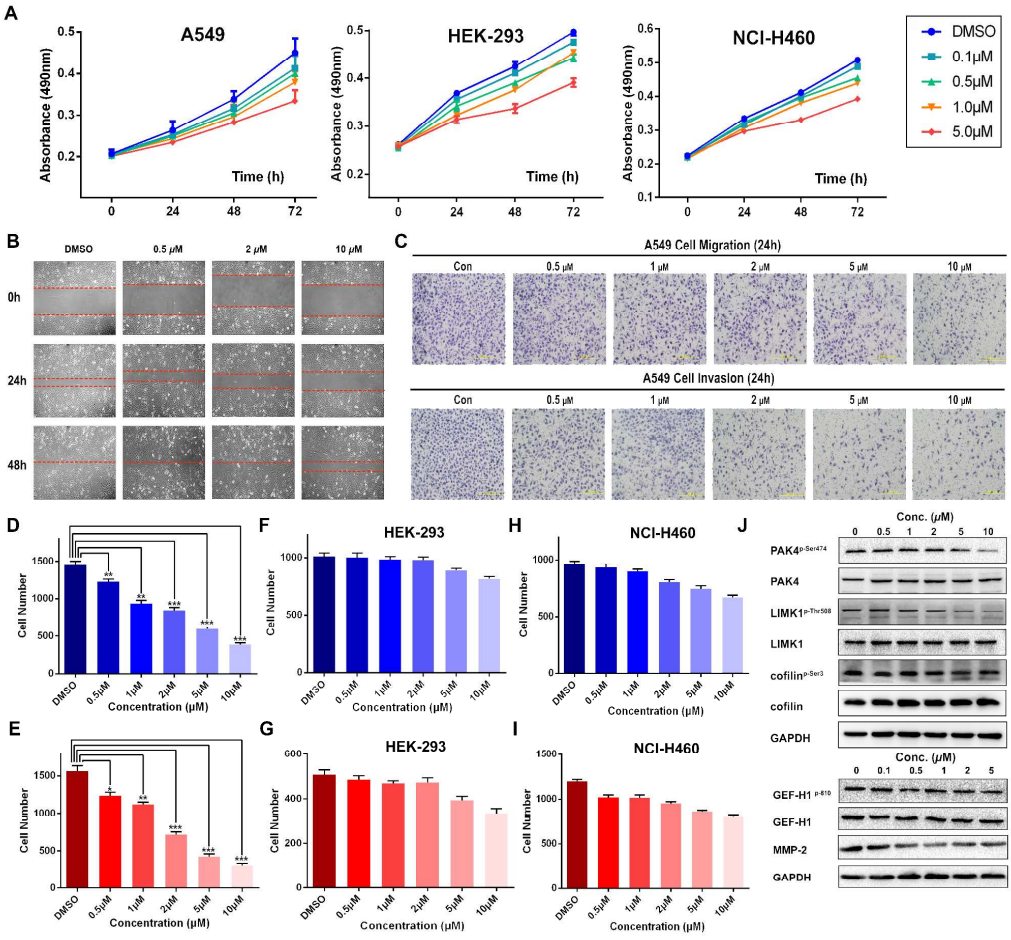

Figure 10. Compound **31** suppresses the migratory and invasive potential of A549 lung cancer cells *via* inhibition of PAK4 kinase activity and its downstream pathways. (A) MTT assay showed the anti-proliferative effect of compound **31** on A549, HEK-293 and NCI-H460 cells. (B) Compound **31** inhibits migration of A549 lung cancer cells in a wound healing assay. (C-F) Transwell assay [-(D)/+ (C) matrigel] was performed to show the effect of indicated concentrations of **31** on A549 lung cancer cells migration (C) and invasion (D). And migrated cells were counted respectively (E-F). The results are presented as the mean ± standard deviation (*, $p < 0.05$; **, $p < 0.01$; ***, $p < 0.001$ vs control). (G-H) Effect of **31** on HEK-293 cells migration (G) and invasion (H). (I-J) Effect of **31** on NCI-H460 cells migration (I)

and invasion (J). Scale bar, 500 μm. (K) Western blot assay showed the effect of compound **31** on the phospho-PAK4 Ser^{474} level and on the phosphorylation levels of PAK4 downstream targets LIMK1 and cofilin. The expression of MMP-2 and the phosphorylation of GEF-H1 were also downregulated by compound **31** treatment in a dose-dependent manner. A549 cells were cultured with vehicle or the indicated concentrations of compound **31** for 24 h, and then proteins were extracted and subjected to analysis.

***In Vitro* Metabolic Stability, CYP450 Inhibition, hERG Inhibition and *in Vivo* Pharmacokinetics Properties.** A preliminary ADMET properties assessment of **31** was conducted to evaluate its potential for further development. The *in vitro* metabolic stability of the compound was assessed in liver microsomes (rat and human) and rat blood plasma. As shown in Table 5, compound **31** possessed moderate microsomal stability and excellent blood plasma stability (for more information, see Supporting Information). Further CYP450 inhibition determination showed that **31** possessed favorable metabolic properties, as the inhibition ratios for the five main CYPs (CYP1A2, 2C9, 2C19, 2D6, and 3A4) were less than 20 % at 10 μM. Previous studies demonstrated that a basic nitrogen (or generally the positive charge feature) would lead to greater activity against human ether-a-go-go-related gene (hERG) channels (Kv11.1).[39] Gratifyingly, the p*K*a of compound **31** (calculated p*K*a = 7.9) was reduced by greater than two units than the early lead (calculated p*K*a = 10.0 for **10a**) and was found to be safe (IC_{50} > 40 μM) when tested in a hERG patch clamp assay for assessing hERG-associated cardiotoxicity. On the basis of these favorable *in*

vitro profiles and excellent aqueous solubility (>10 mg/mL at pH 7.4 and pH 2.0), preliminary pharmacokinetic studies of **31** were performed by administering Sprague-Dawley (SD) rats a 2 mg/kg intravenous (iv) dose of the compound. After the intravenous administration at a dose of 2 mg/kg, **31** exhibited a moderate half-life of 1.46 ± 0.07 h and achieved a maximum concentration (Cmax) of 736 ± 170 ng/mL. The area under the curve (AUC $_{(0-\infty)}$) was 472 ± 23.4 ng·h/mL. It is worth noting that compound **31** exhibited relative high plasma clearance (70.7±3.53 mL/min/kg), which may be due to its high polarity. Further in-depth studies are under way to elucidate the mechanism of action and assess the therapeutic potential of **31** as a new anticancer agent and the results will be reported in due course.

Table 5. Key data for compound **31** (corresponding hydrochloride salt).

Physiochemical Properties					
LogP	$LogD_{7.4}$	p*K*a	DMSO Solubility	Aqueous Solubility at pH 7.4	Aqueous Solubility at pH 2.0
2.54 [a] (2.6 [b])	1.90 [a]	7.93 [a] (7.9 [c])	>30 mM	>10 mg/mL	>10 mg/mL

Liver Microsomal Stability					
Parameters	$T_{1/2}$ (min)	Remaining (%) T = 1 h	Remaining (%) [d] T = 1 h	$CL_{int(mic)}$(μL/min/mg)	$CL_{int(liver)}$(mL/min/kg)
in rat	41.8	36.9 %	97.0 %	33.2	59.7
in human	48.4	41.9 %	102.7 %	28.7	25.8

Cytochrome P450 Inhibition [e]					
Isozyme	CYP1A2	CYP2C9	CYP2C19	CYP2D6	CYP3A4
% inhibition at 10 μM	17.2 %	15.1 %	12.2 %	1.8 %	2.3 %

Stability in Rat Blood Plasma					**hERG Inhibition** [f]	
Parameters	Time Point (min)	% Remaining	Time Point (min)	% Remaining	Parameters	42.0 % inhibition at 40 μM
Compd.**31**	60	110.1 %	120	115.3 %	Compd.**31**	IC_{50} > 40 μM

Pharmacokinetic Parameters (iv administration in SD Rats) [g]						
dose (mg/kg)	C_0 (ng/mL)	Cl (mL/min/kg)	Vss (L/kg)	$T_{1/2}$ (h)	$AUC_{(0-t)}$ (ng·h/mL)	$AUC_{(0-\infty)}$ (ng·h/mL)
2 mg/kg	736±170	70.7±3.53	6.43±0.68	1.46±0.07	465±21.7	472±23.4

[a]Experimental data. [b]The clogP values were calculated using the Qikprop software with default settings (pH = 7.0). [c]Calculated using the Qikprop software. [d]No NADPH regenerating system was added to the sample (replaced by buffer) during the 60

min-incubation. [e]Performed at 10 μM concentration. α-Naphthoflavone (CYP1A2), sulfaphenazole (CYP2C9), ticlopidine (CYP2C19), quinidine (CYP2D6), and ketoconazole (CYP3A4) were used as the positive controls. [f]Measured in hERG-expressing CHO cells using a Qpatch 16× assay. [g]The data are the averages of three independent determinations and reported as the mean ± SD (standard deviation).

CHEMISTRY

The synthesis of 4-aminoimidazole analogs was carried out as shown in Scheme 1. Briefly, N1-alkylation of commercially available nitro-imidazole **42** with the appropriate alkyl halides (methyl iodide or 2-bromopropane) proceeded smoothly followed by palladium-mediated hydrogenation to yield the amino imidazole hydrochloride salts **44a** and **44c** in good yields.[40] Meanwhile, for analogues **44b** and **44d**, an alternate synthetic route was used. 1,4-Dinitro-1*H*-imidazole was obtained by the nitration of **42** following a known general procedure.[41] The treatment of 1,4-dinitroimidazole **46** with primary amines afforded the N1-substituted 4-nitroimidazole **47**, followed by hydrogenation to provide **44b** and **44d**.

Scheme 1. The preparation of 4-aminoimidazole analogs[a]

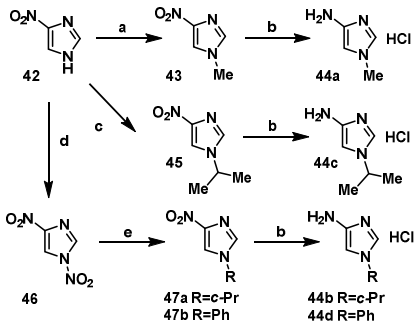

[a]Reagents and conditions: (a) CH_3I, K_2CO_3, MeCN, 65 °C, 12 h; (b) (i) H_2, Pd/C, rt, 8

h; (ii) HCl-EtOH, 0 °C, 1 h; (c) *i*-PrBr, DMF, K_2CO_3, 65 °C, 12 h; (d) HNO_3, Ac_2O, H_2SO_4, 0 °C to rt, 1 h; and (e) RNH_2, MeOH, H_2O, 24 h.

Compounds **10a-d** and **11a-d** containing a scaffold of 6-chloroquinazoline-2, 4-diamine were synthesized as shown in Scheme 2. The synthetic sequence started from 2-amino-5-chlorobenzoic acid. Intermediate **49** was obtained *via* cyclization with urea, which was subjected to chlorination with phosphorus oxychloride in DME to yield the key intermediate **50**. The subsequent condensation of **50** with imidazoles **44a-d** in the presence of *N, N*-diisopropylethylamine produced the corresponding product **51**. The nucleophilic aromatic substitution of intermediates **51a-d** with 4-(*N*-Boc-amino)-piperidine was achieved by heating under acidic condition to provide compounds **52a-d**. The deprotection of **52a-d** under standard conditions produced the desired products **10a-d** in good yield. Compounds **11a-d** were prepared by a method similar to that for compound **10** in similar overall yields.

Scheme 2. The syntheses of 2, 4-diaminoquinazoline derivatives (**10a-d** and **11a-d**)[a]

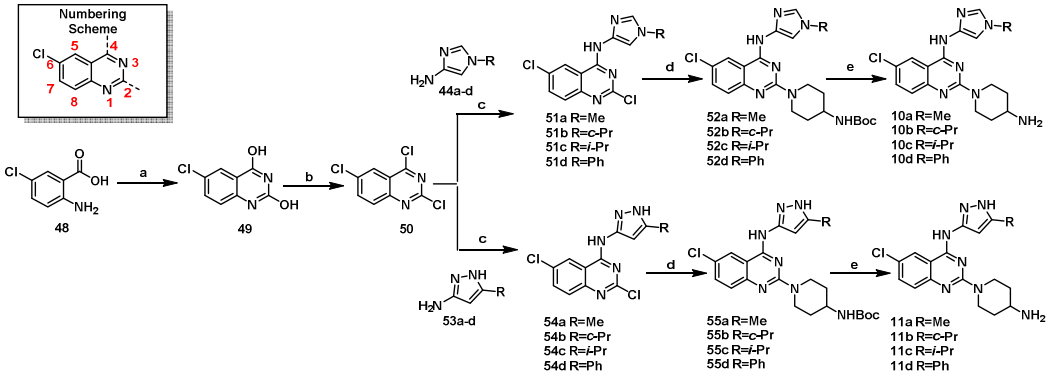

[a]Reagents and conditions: (a) urea, 200 °C; (b) $POCl_3$, *N, N*-dimethylaniline, reflux; (c) DIEA, DMF, 0 °C, 3 h; (d) 4-(*N*-Boc-amino)-piperidine, HCl, EtOH, 120 °C, 15 h; and (e) HCl-EA, DCM, rt, 12 h.

To test the structural-based hypotheses for improving PAK4 selectivity, a novel synthetic strategy was applied to rapidly generate the desired 4-aminoquinazoline-2-carboxamide derivatives (Scheme 3). 2-Amino-5-chlorobenzoic acid reacted with triphosgene and ammonium hydroxide to produce compound **56**, which was acylated by ethyl oxalyl monochloride to afford compound **57**. The ethyl ester **57** was cyclized under basic conditions to give **58** in 86 % yield, which was hydrolyzed in an ethanol/water solution (1:1) with an excess of NaOH (8 equiv), affording the key intermediate **59**. The acid **59** was reacted with $SOCl_2$ to give the dichlorinated product **60**, which could be condensed with various amines to the corresponding amide intermediates (**61**, **63** and **65**) in moderate overall yields. The optimal condition was found to be 1.0 equiv of amine in anhydrous dichloromethane, stirring at -35 °C for 0.5 h. Then, the amides were converted into the intermediates by the replacement of 4-Cl in the quinazoline with the appropriate 1*H*-pyrazol-3-amines in a good yield, which were deprotected under acidic conditions to produce the final compounds (for **13**, **15**, **18**, **19**, and **20**, no deprotection was needed).

Scheme 3. The syntheses of 4-aminoquinazoline-2-carboxamide derivatives (**12-36**)[a]

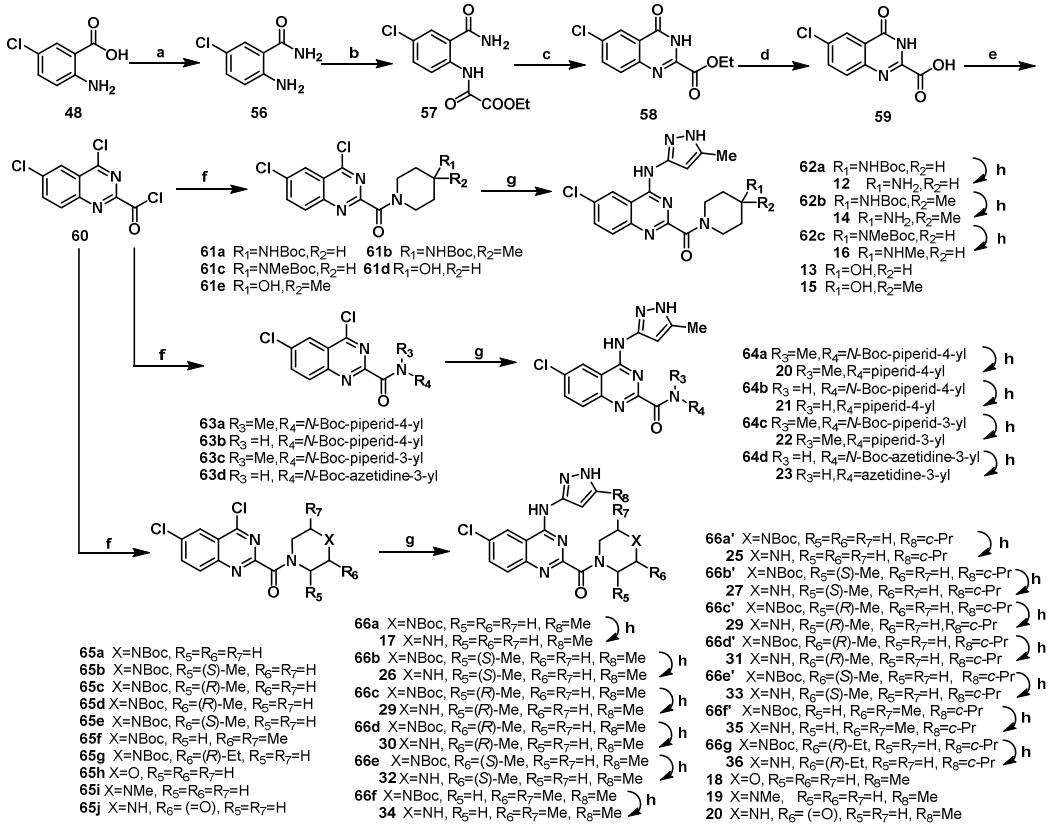

[a]Reagents and conditions: (a) (i) bis(trichloromethyl) carbonate, THF, reflux, 16 h; (ii) 1N NH_3-H_2O, 65 °C, 1 h; (b) ethyl oxalyl monochloride, THF, TEA, 0 °C to rt. 3 h; (c) EtONa, EtOH, 0°C, 3 h; (d) NaOH, H_2O, EtOH, rt. 1 h; (e) $SOCl_2$, chloroform, DMF, reflux, 3 h; (f) amine, DCM, TEA, -35 °C, 0.5 h; (g) 3-amino-5-methylpyrazole or 5-cyclopropyl-1*H*-pyrazol-3-amine, DIEA, KI, DMF, 65 °C, 8 h; and (h) HCl-EA, DCM, rt, 6 h.

Compounds **37-41** were synthesized in a similar manner starting from the corresponding acid materials, **67a-e**, in a moderate overall yield (Scheme 4). All compounds were characterized by ^{1}H NMR, ^{13}C NMR and HRMS, and their purity was determined by reverse phase HPLC (see the Supporting Information for details).

Scheme 4. The syntheses of compounds **37-41**[a]

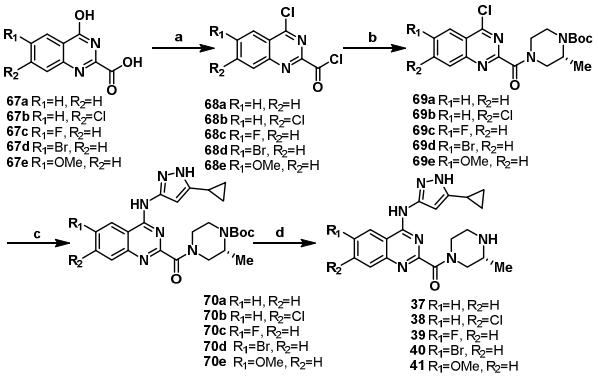

[a] Reagents and conditions: (a) $SOCl_2$, chloroform, DMF, reflux, 3 h; (b) *tert*-butyl (*R*)-2-methylpiperazine-1-carboxylate, DCM, TEA, -35 °C, 0.5 h; (c) 5-cyclopropyl-1*H*-pyrazol-3-amine, DIEA, KI, DMF, 65 °C, 8 h; and (d) HCl-EA, DCM, rt, 6 h.

CONCLUSIONS

In summary, starting from the 2, 4-diaminoquinazoline scaffold compound **10a**, a series of novel 4-aminoquinazoline-2-carboxamide derivatives was designed and synthesized as selective and potent PAK4 inhibitors by utilizing highly efficient structure-based design strategies targeting key residues differences between PAK1 and PAK4. The optimized compound **31** demonstrates a striking selectivity for PAK4 over PAK1 (346-fold). As expected, the X-ray structure of **31** bound to PAK4 agrees well with the above-described design hypothesis. Our study also demonstrates that the selectivity and potency of PAK4 inhibitors can be improved by targeting the DFG motif and several other distinguishing features of the ATP-binding pocket. Furthermore, compound **31** possesses good kinome selectivity, favorable physicochemical properties, and moderate ADME properties, both *in vitro* and *in vivo*. Moreover, this compound inhibited the migration and invasion of A549 tumor

cells by regulating the PAK4-directed downstream signaling pathways *in vitro*. Taken together, compound **31** may serve as a new lead compound for anticancer drug discovery, as well as a valuable research probe for further biological investigation on group II PAKs. The results from this study also provides molecular insights into the development of novel selective PAK4 kinase inhibitors.

EXPERIMENTAL SECTION

General Methods for Chemistry. Commercially available chemicals were used as purchased without further purification. Solvents were purified and stored according to standard procedures. All reactions were monitored by thin-layer chromatography (TLC), and silica gel plates with fluorescence F-254 were used and visualized with UV light. Column chromatography was carried out on silica gel (100-200 mesh). The melting points were determined on a Buchi melting point B-540 apparatus and are uncorrected. The NMR spectra were measured on a Bruker Avance □-600 and/or Bruker Avance □-400 instruments (600 or 400 MHz for ^{1}H and 150 or 100 MHz for ^{13}C). Chemical shifts are expressed as δ units using tetramethylsilane as the external standard (in NMR description, s, singlet; d, doublet; t, triplet; q, quartet; m, multiplet; and br, broad peak). All coupling constants (*J*) are reported in Hertz. LC-MS analysis was performed on Agilent 1200 LC-MS using ESI mode. High-resolution mass spectra (HRMS) were performed on Agilent 6530 accurate-mass Q-TOF LC-MS system. All of the final compounds were purified to >95 % purity, as determined by high-performance liquid chromatography (HPLC). This analysis was performed on a Waters Breeze system (Waters 1525, binary HPLC pump) equipped with an UV

detector (Waters 2487, dual λ absorbance detector) and a WondaSil C-18 Superb column (5 μm, 4.6 mm × 250 mm) using a mobile phase of 60 % acetonitrile in water containing 0.05 % TFA. The flow-rate was 0.6 mL/min, and the injection volume was 20 μL. Peaks were detected at 254 nm. The retention times (RT) are in minutes, and the purity was calculated as percentage of total area.

2-(4-Aminopiperidin-1-yl)-6-chloro-*N*-(1-methyl-1*H*-imidazol-4-yl)quinazolin-4-amine hydrochloride (10a). 2 M HCl in ethyl acetate (4 mL) was added to a solution of **52a** (152 mg, 0.33 mmol) in dichloromethane (10 mL). The mixture was stirred for 12 h at room temperature, and then, the resulting solid was filtered and dried to give the title compound (120 mg, 91 % yield) as a white solid. ^{1}H NMR (400 MHz, DMSO-d_6) δ 8.89 (d, J = 1.9 Hz, 1H), 8.41 (br, 3H), 8.38 (s, 1H), 8.19 (d, J = 8.8 Hz, 1H), 7.91(dd, J = 2.2, 9.0 Hz, 1H), 7.58 (d, J = 1.3 Hz, 1H), 4.75-4.72 (m, 2H), 3.85 (s, 3H), 3.42-3.41 (m, 1H), 3.36-3.30 (m, 2H), 2.14-2.11 (m, 2H), 1.71-1.63 (m, 2H). ^{13}C NMR (100 MHz, DMSO-d_6) δ 157.2, 151.8, 140.0, 135.9, 134.3, 130.1, 129.4, 124.5, 120.4, 114.0, 111.2, 49.0, 44.4, 35.9, 29.7. HRMS (ESI, m/z) calcd for $C_{17}H_{21}ClN_7$ $[M+H]^+$, 358.1541; found 358.1547. R_f= 0.12 (DCM/MeOH, 10/1, v/v). Retention time: 3.95 min, 95.24 % purity.

2-(4-Aminopiperidin-1-yl)-6-chloro-*N*-(1-cyclopropyl-1*H*-imidazol-4-yl)quinazolin-4-amine hydrochloride (10b). Compound **10b** was prepared in a similar manner as compound **10a**, using **44b** (R = *c*-Pr) instead of **44a** (R = Me). Light-yellow solid (yield 37 %). ^{1}H NMR (600 MHz, DMSO-d_6) δ 8.90 (d, J = 1.7 Hz, 1H), 8.45 (br, 3H), 8.43 (s, 1H), 8.24 (d, J = 8.9 Hz, 1H), 7.92(dd, J = 2.0, 8.9 Hz, 1H), 7.63 (s, 1H),

4.75 (br, 2H), 3.77-3.74 (m, 1H), 3.44-3.41 (m, 1H), 3.40-3.36 (m, 2H), 2.13-2.11 (m, 2H), 1.73-1.67 (m, 2H), 1.11-1.03 (m, 4H). ^{13}C NMR (100 MHz, DMSO-d_6) δ 157.2, 151.7, 139.9, 135.9, 134.3, 130.7, 129.5, 124.5, 120.3, 113.5, 111.1, 49.0, 47.1, 44.3, 30.6, 29.7, 6.74. HRMS (ESI, m/z) calcd for $C_{19}H_{23}ClN_7$ $[M+H]^+$, 384.1698; found 384.1699. R_f =0.18 (DCM/MeOH, 10/1, v/v). Retention time: 3.37 min, 97.52 % purity.

2-(4-Aminopiperidin-1-yl)-6-chloro-*N*-(1-isopropyl-1*H*-imidazol-4-yl)quinazolin-4-amine hydrochloride (10c). Compound **10c** was prepared in a similar manner as compound **10a**, using **44c** (R = *i*-Pr) instead of **44a** (R = Me). Off-white solid (yield 33 %). ^{1}H NMR (400 MHz, DMSO-d_6) δ 8.91 (d, J = 1.9 Hz, 1H), 8.60 (s, 1H), 8.42 (br, 3H), 8.22 (d, J = 9.0 Hz, 1H), 7.92 (dd, J = 2.2, 9.0 Hz, 1H), 7.77 (d, J = 1.3, 1H), 4.75-4.72 (m, 2H), 4.68-4.60 (m, 1H), 3.42-3.41 (m, 1H), 3.37-3.31 (m, 2H), 2.11-2.09 (m, 2H), 1.72-1.65 (m, 2H), 1.51 (s, 3H), 1.50 (s, 3H). ^{13}C NMR (100 MHz, DMSO-d_6) δ 157.5, 151.8, 140.2, 136.0, 132.4, 130.4, 129.4, 124.5, 120.5, 111.6, 111.2, 52.0, 49.0, 47.1, 44.3, 29.6, 23.0. HRMS (ESI, m/z) calcd for $C_{19}H_{23}ClN_7$ $[M + H]^+$, 386.1854, found 386.1854. R_f= 0.21 (DCM/MeOH, 10/1, v/v). Retention time: 3.84 min, 98.53 % purity.

2-(4-Aminopiperidin-1-yl)-6-chloro-*N*-(1-phenyl-1*H*-imidazol-4-yl)quinazolin-4-amine hydrochloride (10d). Compound **10d** was prepared in a similar manner as compound **10a**, using **44d** (R = Ph) instead of **44a** (R = Me). White solid (yield 31 %). ^{1}H NMR (600 MHz, DMSO-d_6) δ 13.34 (br, 1H), 11.81 (br, 1H), 8.93 (d, J = 1.4 Hz, 1H), 8.48 (s, 1H), 8.44 (br, 3H), 8.26 (d, J = 8.9 Hz, 1H), 7.98 (s, 1H), 7.92 (dd, J

= 1.8, 8.9 Hz, 1H), 7.69 (d, *J* = 7.9, 1H), 7.59 (t, *J* = 7.7, 1H), 7.45 (t, *J* = 7.4, 1H), 4.83 (br, 2H), 3.44 (m, 1H), 3.42-3.40 (m, 2H), 2.15-2.13(m, 2H), 1.76-1.70 (m, 2H). ^{13}C NMR (100 MHz, D_2O) *δ* 159.0, 151.5, 136.7, 130.7, 130.4, 130.2, 123.3, 122.1, 119.1, 110.4, 105.3, 48.9, 47.5, 43.7, 28.9. HRMS (ESI, m/z) calcd for $C_{22}H_{23}ClN_7$ $[M + H]^+$; 420.1698; found 420.1704. R_f= 0.32 (DCM/MeOH, 10/1, v/v). Retention time: 4.04 min, 100 % purity.

2-(4-Aminopiperidin-1-yl)-6-chloro-*N*-(5-methyl-1*H*-pyrazol-3-yl)quinazolin-4-amine hydrochloride (11a). Compound **11a** was prepared in a similar manner as compound **10a**, using **53a** (R = Me) instead of **44a**. White solid (yield 41 %). ^{1}H NMR (400 MHz, DMSO-d_6) *δ* 13.20 (br, 1H), 11.47 (s, 1H), 8.84 (d, *J* = 2.0 Hz, 1H), 8.43 (br, 3H), 8.23 (d, *J* = 9.0 Hz, 1H), 7.91 (dd, *J* = 2.1, 8.9 Hz, 1H), 6.41 (s, 1H), 4.80-4.76 (m, 2H), 3.43-3.32 (m, 3H), 2.31 (s, 3H), 2.14-2.11 (m, 2H), 1.71-1.63 (m, 2H). ^{13}C NMR (100 MHz, DMSO-d_6) δ 156.7, 151.7, 145.8, 139.8, 139.6, 135.5, 129.3, 124.3, 120.2, 111.5, 98.5, 47.2, 44.2, 29.6, 11.3. HRMS (ESI, m/z) calcd for $C_{17}H_{21}ClN_7$ $[M+H]^+$, 358.1541; found 358.1542. R_f= 0.13 (DCM/MeOH, 10/1, v/v). Retention time: 3.88 min, 96.28 % purity.

2-(4-Aminopiperidin-1-yl)-6-chloro-*N*-(5-cyclopropyl-1*H*-pyrazol-3-yl)quinazolin-4-amine hydrochloride (11b). Compound **11b** was prepared in a similar manner as compound **10a**, using **53b** (R = *c*-Pr) instead of **44a**. White solid (yield 43 %). ^{1}H NMR (400 MHz, DMSO-d_6) *δ* 13.30 (br, 1H), 11.49 (d, *J* = 2.0 Hz, 1H), 8.47 (br, 3H), 8.81 (d, 1H), 8.26 (d, *J* = 9.0 Hz, 1H), 7.89 (dd, *J* = 2.1, 8.9 Hz, 1H), 6.28 (s, 1H), 4.79-4.77 (m, 2H), 3.43-3.32 (m, 3H), 2.12-2.09 (m, 2H), 2.00-1.95 (m, 1H),

1.71-1.64 (m, 2H), 1.01-0.97 (m, 2H), 0.71-0.67 (m, 2H). ^{13}C NMR (100 MHz, DMSO-d_6) δ 156.7, 151.6, 147.0, 145.8, 139.6, 135.5, 129.4, 124.3, 120.2, 111.4, 95.3, 47.2, 44.2, 29.6, 8.7, 7.3. HRMS (ESI, m/z) calcd for $C_{19}H_{23}ClN_7$ $[M+H]^+$, 384.1698; found 384.1711. R_f= 0.17 (DCM/MeOH, 10/1, v/v). Retention time: 3.99 min, 100 % purity.

2-(4-Aminopiperidin-1-yl)-6-chloro-*N*-(5-isopropyl-1*H*-pyrazol-3-yl)quinazolin-4-amine hydrochloride (11c). Compound **11c** was prepared in a similar manner as compound **10a**, using **53c** (R = *i*-Pr) instead of **44a**. White solid (yield 32 %). ^{1}H NMR (400 MHz, DMSO-d_6) δ 13.15 (br, 1H), 11.54 (s, 1H), 8.83 (d, J = 1.8 Hz, 1H), 8.37 (br, 3H), 8.19 (d, J = 8.9 Hz, 1H), 7.92 (dd, J = 2.0, 8.9 Hz, 1H), 6.45 (s, 1H), 4.77 (d, J = 12.8 Hz, 2H), 3.51-3.33 (m, 3H), 3.05-2.98 (m, 1H), 2.11-2.09 (m, 2H), 1.72-1.66 (m, 2H), 1.27(s, 3H), 1.25 (s, 3H). ^{13}C NMR (100 MHz, D_2O) δ 156.4, 151.0, 137.7, 135.8, 130.5, 122.6, 118.8, 110.1, 48.9, 47.5, 43.7, 28.9, 25.6, 21.3. HRMS (ESI, m/z) calcd for $C_{19}H_{23}ClN_7$ $[M+H]^+$, 386.1854; found 386.1861. R_f= 0.20 (DCM/MeOH, 10/1, v/v). Retention time: 3.90 min, 96.16 % purity.

2-(4-Aminopiperidin-1-yl)-6-chloro-*N*-(5-phenyl-1*H*-pyrazol-3-yl)quinazolin-4-amine hydrochloride (11d). Compound **11d** was prepared in a similar manner as compound **10a**, using **53d** (R = Ph) instead of **44a**. White solid (yield 27 %). ^{1}H NMR (400 MHz, DMSO-d_6) δ 13.29 (br, 1H), 11.66 (s, 1H), 8.87 (d, J = 1.80 Hz, 1H) , 8.40 (br, 3H), 8.25 (d, J = 9.0 Hz, 1H), 7.94 (dd, J = 2.0, 8.9 Hz, 1H), 7.78 (d, J = 7.4 Hz, 2H), 7.51 (t, J = 7.5 Hz, 2H), 7.41 (t, J = 7.3 Hz, 1H), 7.05 (s, 1H), 4.83-4.80 (m, 2H), 3.45-3.36 (m, 3H), 2.15-2.12 (m, 2H), 1.75-1.67 (m, 2H). ^{13}C NMR (100 MHz,

DMSO-d_6) δ 156.9, 151.6, 146.5, 143.2, 139.7, 135.6, 129.6, 129.4, 128.9, 125.5, 124.3, 120.2, 111.4, 96.8, 47.2, 44.3, 29.7. HRMS (ESI, m/z) calcd for $C_{22}H_{23}ClN_7$ $[M+H]^+$, 420.1698; found 420.1701. R_f = 0.23 (DCM/MeOH, 10/1, v/v). Retention time: 3.96 min, 96.67 % purity.

Compounds **12-41** were synthesized using a similar procedure with yields in the range 12-28 % (8 steps; for **13**, **15**, **18**, **19**, **20**, no Boc deprotection was needed).

(4-Aminopiperidin-1-yl)(6-chloro-4-((5-methyl-1*H*-pyrazol-3-yl)amino)quinazolin-2-yl)methanone hydrochloride (12). Off-white solid (yield 27 %). ^{1}H NMR (400 MHz, DMSO-d_6) δ 11.73 (br, 1H), 9.05 (d, J = 2.0 Hz, 1H), 8.42 (br, 3H), 8.03 (dd, J = 2.1, 8.9 Hz, 1H), 7.92 (d, J = 9.0 Hz, 1H), 6.53 (s, 1H), 4.50-4.47 (m, 1H), 3.86-3.83 (m, 1H), 3.38-3.30 (m, 1H), 3.21-3.15 (m, 1H), 3.03-2.97 (m, 1H), 2.34 (s, 3H), 2.11-2.08 (m, 1H), 1.93-1.90 (m, 1H), 1.65-1.53 (m, 2H). ^{13}C NMR (100 MHz, DMSO-d_6) δ 162.1, 157.1, 155.0, 145.5, 143.1, 141.1, 135.9, 133.0, 126.5, 124.3, 115.4, 98.7, 47.6, 44.7, 30.4, 29.5, 11.4. HRMS (ESI, m/z) calcd for $C_{18}H_{21}ClN_7O$ $[M+H]^+$, 386.1491; found 386.1500. R_f = 0.10 (DCM/MeOH, 5/1, v/v). Retention time: 3.91 min, 96.28 % purity.

(6-Chloro-4-((5-methyl-1*H*-pyrazol-3-yl)amino)quinazolin-2-yl)(4-hydroxypiperidin-1-yl)methanone (13). Off-white solid (yield 19 %). ^{1}H NMR (400 MHz, DMSO-d_6) δ 12.29 (s, 1H), 10.69 (s, 1H), 8.88 (s, 1H), 7.88 (dd, J = 1.8, 8.9 Hz, 1H), 7.79 (d, J = 8.8 Hz, 1H), 6.56 (s, 1H), 4.83 (d, J = 4.0 Hz, 1H), 4.06-4.02 (m, 1H), 3.77-3.72 (m, 1H), 3.39-3.32 (m, 1H), 3.26-3.21 (m, 1H), 3.07-3.02 (m, 1H), 2.27 (s, 3H), 1.84-1.81 (m, 1H), 1.71-1.67 (m, 1H), 1.41-1.30 (m, 2H). ^{13}C NMR (100 MHz,

DMSO-d_6) δ 165.5, 159.1, 157.1, 148.4, 138.8, 134.1, 131.3, 130.3, 123.3, 115.5, 98.3, 65.9, 44.0, 38.8, 35.0, 34.3, 11.3. HRMS (ESI, m/z) calcd for $C_{18}H_{20}ClN_6O_2$ $[M+H]^+$, 387.1331; found 387.1334. R_f = 0.60 (DCM/MeOH, 5/1, v/v). Retention time: 4.57 min, 96.49 % purity.

(4-Amino-4-methylpiperidin-1-yl)(6-chloro-4-((5-methyl-1*H*-pyrazol-3-yl)amino)quinazolin-2-yl)methanone hydrochloride (14). Off-white solid (yield 23 %). ^{1}H NMR (400 MHz, DMSO-d_6) δ 11.94 (br, 1H), 9.08 (d, J = 1.9 Hz, 1H), 8.52 (br, 3H), 8.05 (dd, J = 2.1, 8.9 Hz, 1H), 7.95 (d, J = 8.9 Hz, 1H), 6.56 (s, 1H), 4.05-4.01 (m, 1H), 3.77-3.73 (m, 1H), 3.61-3.56 (m, 1H), 3.46-3.42 (m, 1H), 2.34 (s, 3H), 1.92-1.70 (m, 4H), 1.38 (s, 3H). ^{13}C NMR (100 MHz, DMSO-d_6) δ 162.0, 157.2, 154.9, 145.5, 142.9, 141.1, 135.9, 133.0, 126.3, 124.3, 115.4, 98.8, 52.3, 42.4, 37.8, 35.5, 34.6, 23.5, 11.3. HRMS (ESI, m/z) calcd for $C_{19}H_{23}ClN_7O$ $[M+H]^+$, 400.1647; found 400.1655. R_f = 0.13 (DCM/MeOH, 5/1, v/v). Retention time: 3.90 min, 95.57 % purity.

(6-Chloro-4-((5-methyl-1*H*-pyrazol-3-yl)amino)quinazolin-2-yl)(4-hydroxy-4-m ethylpiperidin-1-yl)methanone (15). Off-white solid (yield 16 %). ^{1}H NMR (400 MHz, DMSO-d_6) δ 12.28 (s, 1H), 10.68 (s, 1H), 8.88 (s, 1H), 7.88 (dd, J = 2.1, 8.9 Hz, 1H), 7.79 (d, J = 8.9 Hz, 1H), 6.55 (s, 1H), 4.46 (s, 1H), 4.11-4.08 (m, 1H), 3.24-3.16 (m, 2H), 3.09-3.04 (m, 1H), 2.27 (s, 3H), 1.60-1.38 (m, 4H), 1.16 (s, 3H). ^{13}C NMR (100 MHz, DMSO-d_6) δ 165.5, 159.2, 157.1, 148.5, 138.9, 134.1, 131.2, 130.3, 123.2, 115.5, 98.3, 66.7, 45.8, 43.2, 39.1, 38.4, 37.8, 30.4, 11.3, 8.9. HRMS

(ESI, m/z) calcd for $C_{19}H_{22}ClN_6O_2$ $[M+H]^+$, 401.1487; found 401.1501. R_f = 0.63 (DCM/MeOH, 5/1, v/v). Retention time: 4.37 min, 95.16 % purity.

(6-Chloro-4-((5-methyl-1*H*-pyrazol-3-yl)amino)quinazolin-2-yl)(4-(methylamino)piperidin-1-yl)methanone hydrochloride (16). Light-yellow solid (yield 26 %). ^{1}H NMR (400 MHz, DMSO-d_6) δ 11.82 (br, 2H), 9.52-9.44 (m, 2H), 9.07 (d, J = 1.8 Hz, 1H), 8.03 (dd, J = 2.0, 8.9 Hz, 1H), 7.93 (d, J = 8.9 Hz, 1H), 6.54 (s, 1H), 4.55-4.52 (m, 1H), 3.92-3.89 (m, 1H), 3.31-3.22 (m, 1H), 3.17-3.11 (m, 1H), 2.99-2.93 (m, 1H), 2.50 (s, 3H), 2.34 (s, 3H), 2.21-2.18 (m, 1H), 2.02-1.99 (m, 1H), 1.70-1.60 (m, 2H). ^{13}C NMR (100 MHz, DMSO-d_6) δ 162.5, 157.1, 155.5, 145.8, 143.7, 140.8, 135.7, 132.7, 126.9, 124.1, 115.4, 98.6, 55.0, 44.7, 29.6, 28.5, 27.6, 11.4. HRMS (ESI, m/z) calcd for $C_{19}H_{23}ClN_7$ $[M+H]^+$, 400.1647; found 401.1650. R_f = 0.10 (DCM/MeOH, 5/1, v/v). Retention time: 3.98 min, 95.79 % purity.

(6-Chloro-4-((5-methyl-1*H*-pyrazol-3-yl)amino)quinazolin-2-yl)(piperazin-1-yl) methanone hydrochloride (17). 2 M HCl in ethyl acetate (4 mL) was added to a solution of *tert*-butyl 4-(6-chloro-4-((5-methyl-1*H*-pyrazol-3-yl)amino)quinazoline -2-carbonyl)piperazine-1-carboxylate (**66a**, 145 mg, 0.35 mmol) in dichloromethane (5 mL). The mixture was stirred for 6 h at room temperature, and then, the resulting solid was filtered and dried to give the title compound (120 mg, 91 % yield) as a white solid. ^{1}H NMR (400 MHz, DMSO-d_6) δ 11.47 (br, 1H), 9.59 (s, 2H), 9.01 (s, 1H), 8.02-8.00 (m,1H), 7.91 (dd, J = 2.6, 8.8 Hz, 1H), 6.56 (s, 1H), 3.93-3.91 (m, 2H), 3.71 (s, 2H), 3.23 (s, 2H), 3.09 (s, 2H), 2.32 (s, 3H). ^{13}C NMR (100 MHz, DMSO-d_6) δ 163.0, 157.1, 155.0, 145.7, 144.4, 140.9, 135.6, 132.8, 127.6, 124.0,

115.5, 98.6, 43.4, 43.1, 42.7, 38.8, 11.4. HRMS (ESI, m/z) calcd for $C_{17}H_{19}ClN_7O$ $[M+H]^+$, 372.1334 ; found 372.1333. R_f = 0.21 (DCM/MeOH, 5/1, v/v). Retention time: 4.82 min, 95.04 % purity.

(6-Chloro-4-((5-methyl-1*H*-pyrazol-3-yl)amino)quinazolin-2-yl)(morpholino)methanone (18). White solid (yield 13 %). ^{1}H NMR (400 MHz, DMSO-d_6) δ 12.28 (s, 1H), 10.71 (s, 1H), 8.88 (d, J = 1.9 Hz, 1H), 7.88 (dd, J = 2.1, 8.9 Hz, 1H), 7.79 (d, J = 8.9 Hz, 1H), 6.57 (s, 1H), 3.68-3.65 (m, 4H), 3.54-3.52 (m, 2H), 3.30-3.28 (m, 2H), 2.28 (s, 3H). ^{13}C NMR (100 MHz, DMSO-d_6) δ 165.7, 158.4, 157.1, 148.4, 147.6, 138.8, 134.2, 131.4, 130.3, 123.2, 115.5, 98.4, 66.8, 66.5, 47.0, 41.7, 11.3. HRMS (ESI, m/z) calcd for $C_{17}H_{18}ClN_6O_2$ $[M+H]^+$, 373.1174; found 373.1176. R_f = 0.43 (DCM/MeOH, 5/1, v/v). Retention time: 4.55 min, 96.72 % purity.

(6-Chloro-4-((5-methyl-1*H*-pyrazol-3-yl)amino)quinazolin-2-yl)(4-methylpiperazin-1-yl)methanone (19). White solid (yield 22%). ^{1}H NMR (400 MHz, DMSO-d_6) δ 12.28 (s, 1H), 10.71(s, 1H), 8.89 (d, J = 1.8 Hz, 1H), 7.88 (dd, J = 2.0, 8.9 Hz, 1H), 7.79 (d, J = 8.9 Hz, 1H), 6.59 (s, 1H), 3.65-3.63 (m, 2H), 3.26-3.23 (m, 2H), 3.40-3.37 (m, 2H), 2.28 (s, 3H), 2.27-2.22 (m, 2H), 2.20 (s, 3H). ^{13}C NMR (100 MHz, DMSO-d_6) δ 165.6, 158.7, 157.1, 148.4, 147.6, 138.7, 134.1, 131.3, 130.3, 123.2, 115.5, 98.4, 55.2, 54.7, 46.3, 46.2, 41.2, 11.2. HRMS (ESI, m/z) calcd for $C_{18}H_{21}ClN_7O$ $[M+H]^+$, 386.1491; found 386.1502. R_f=0.20 (DCM/MeOH, 5/1, v/v). Retention time: 3.91 min, 95.48 % purity.

4-(6-Chloro-4-((5-methyl-1*H*-pyrazol-3-yl)amino)quinazoline-2-carbonyl)piperazin-2-one (20). Yellow solid (yield 12 %). ^{1}H NMR (600 MHz, DMSO-d_6) δ 12.30 (s,

1H), 10.70 (m, 1H), 8.90-8.88 (m, 1H), 8.18-8.15 (m, 1H), 7.90 (d, *J* = 8.8 Hz, 1H), 7.80 (d, *J* = 8.9 Hz, 1H), 6.56 (s, 1H), 4.16-3.90 (m, 2H), 3.85-3.45 (m, 2H), 3.32-3.17 (m, 2H), 2.27 (s, 3H). ^{13}C NMR (150 MHz, DMSO-d_6) δ 166.3, 165.6, 158.0, 157.3, 148.3, 147.5, 138.9, 134.3, 131.6, 130.4, 123.3, 115.7, 98.4, 49.6, 45.6, 43.2, 40.9, 40.5, 38.6, 11.3. HRMS (ESI, m/z) calcd for $C_{17}H_{16}ClN_7O_2$, $[M+H]^+$, 386.1127; found 386.1118. R_f= 0.30 (DCM/MeOH, 10/1, v/v). Retention time: 4.29 min, 96.01 % purity.

6-Chloro-*N*-methyl-4-((5-methyl-1*H*-pyrazol-3-yl)amino)-*N*-(piperidin-4-yl)quinazoline-2-carboxamide hydrochloride (21). Light-yellow solid (yield 21 %). ^{1}H NMR (400 MHz, DMSO-d_6) δ 11.35 (br, 1H), 8.98-8.81 (m, 3H), 7.99 (t, *J* = 9.1 Hz, 1H), 7.89 (d, *J* =7.2 Hz, 1H), 6.55-6.41 (m, 1H), 4.66-4.60 (m, 1H), 3.88-3.82 (m, 1H), 3.40-3.37 (m, 1H), 3.12-3.07 (m, 1H), 2.90-2.80 (m, 3H), 2.77-2.68 (m, 1H), 2.29 (s, 3H), 2.09-2.07(m, 2H), 1.86-1.78 (m, 2H). ^{13}C NMR (100 MHz, DMSO-d_6) δ 163.8, 158.1, 157.0, 155.7, 145.6, 140.6, 135.8, 132.7, 126.3, 124.2, 115.5, 99.1, 52.8, 49.0, 43.0, 42.4, 31.3, 27.4, 26.2, 25.1, 11.3. HRMS (ESI, m/z) calcd for $C_{19}H_{23}ClN_7O$ $[M+H]^+$, 400.1647; found 400.1649. R_f= 0.25 (DCM/MeOH, 5/1, v/v). Retention time: 3.99 min, 97.40 % purity.

6-Chloro-4-((5-methyl-1*H*-pyrazol-3-yl)amino)-*N*-(piperidin-4-yl)quinazoline-2-carboxamide hydrochloride (22). Off-white solid (yield 19 %). ^{1}H NMR (400 MHz, DMSO-d_6) δ 12.55 (br, 1H), 9.29 (s, 1H), 9.17-9.07 (m, 3H), 8.13 (dd, *J* = 2.0, 8.9 Hz, 1H), 8.06 (d, *J* = 8.9 Hz, 1H), 6.68 (s, 1H), 4.15-4.07 (m, 1H), 3.34-3.31 (m, 2H), 3.07-3.02 (m, 2H), 2.35 (s, 3H), 2.03-1.89 (m, 4H). ^{13}C NMR (100 MHz, DMSO-d_6)

δ 159.3, 153.5, 147.3, 146.9, 143.9, 141.0, 136.9, 134.3, 128.7, 125.4, 116.4, 98.0, 45.6, 42.4, 28.0, 11.2. HRMS (ESI, m/z) calcd for $C_{18}H_{21}ClN_7O$ $[M+H]^+$, 386.1491; found 386.1492. R_f= 0.21 (DCM/MeOH, 5/1, v/v). Retention time: 4.57 min, 95.13 % purity.

6-Chloro-*N*-methyl-4-((5-methyl-1*H*-pyrazol-3-yl)amino)-*N*-(piperidin-3-yl)quinazoline-2-carboxamide hydrochloride (23). Light-yellow solid (yield 15 %). ^{1}H NMR (400 MHz, DMSO-d_6) δ 11.60 (br, 1H), 9.62-9.47 (m, 1H), 9.22-8.94 (m, 1H), 9.03 (dd, J = 1.6, 11.0 Hz, 1H), 8.02 (dd, J =1.9, 9.0 Hz, 1H), 7.95-7.90 (m, 1H), 6.57-6.48 (m, 1H), 4.76-3.95 (m, 1H), 3.30-3.05 (m, 3H), 2.95-2.87 (m, 3H), 2.83-2.65 (m, 1H), 2.31 (s, 3H), 1.96-1.46 (m, 4H). ^{13}C NMR (100 MHz, DMSO-d_6) δ 164.2, 157.7, 155.5, 145.5, 143.3, 141.0, 135.7, 132.8, 126.7, 124.2, 115.6, 98.8, 51.9, 48.3, 44.9, 43.8, 42.9, 42.4, 31.8, 27.6, 26.4, 25.2, 21.8, 21.3, 11.3. HRMS (ESI, m/z) calcd for $C_{19}H_{23}ClN_7O$ $[M+H]^+$, 400.1647; found 400.1650. R_f = 0.36 (DCM/MeOH, 5/1, v/v). Retention time: 3.92 min, 95.14 % purity.

***N*-(Azetidin-3-yl)-6-chloro-4-((5-methyl-1*H*-pyrazol-3-yl)amino)quinazoline-2-carboxamide hydrochloride (24).** Yellow solid (yield 17 %). ^{1}H NMR (400 MHz, DMSO-d_6) δ 11.96 (br, 1H), 9.70-9.04 (m, 3H), 8.26 (s, 1H), 8.07-7.96 (m, 2H), 6.82 (s, 1H), 4.92-4.86 (m, 1H), 4.58-4.53 (m, 1H), 4.24-4.17 (m, 2H), 3.96-3.94 (m, 1H), 3.18-3.16 (m, 1H), 2.32 (d, J = 2.4 Hz, 3H). ^{13}C NMR (100 MHz, DMSO-d_6) δ 160.9, 154.0, 148.7, 147.1, 145.5, 140.8, 136.2, 133.9, 129.7, 124.9, 116.6, 98.1, 51.8, 49.9, 44.9, 42.0, 11.3. HRMS (ESI, m/z) calcd for $C_{16}H_{17}ClN_7O$, $[M+H]^+$, 358.1178; found 358.1178. R_f=0.21 (DCM/MeOH, 5/1, v/v). Retention time: 3.90 min, 95.03 % purity.

(6-Chloro-4-((5-cyclopropyl-1*H*-pyrazol-3-yl)amino)quinazolin-2-yl)(piperazin-1-yl)methanone hydrochloride (25). Off-white solid (yield 26 %). ^{1}H NMR (400 MHz, DMSO-d_6) δ 11.52 (br, 1H), 9.57 (s, 2H), 9.00 (d, J = 1.9 Hz, 1H), 8.01 (dd, J = 2.1, 8.9 Hz, 1H), 7.92 (d, J = 8.9 Hz, 1H), 6.46 (s, 1H), 3.93-3.91 (m, 2H), 3.75-3.72 (m, 2H), 3.23 (s, 2H), 3.10 (s, 2H), 2.04-1.97 (m, 1H), 1.02-0.97 (m, 2H), 0.80-0.76 (m, 2H). ^{13}C NMR (100 MHz, DMSO-d_6) δ 162.0, 157.0, 153.8 148.3, 145.2, 143.0, 136.1, 133.3, 126.6, 124.4, 115.4, 95.8, 49.0, 43.5, 43.0, 42.6, 39.0, 8.8, 7.4. HRMS (ESI, m/z) calcd for $C_{19}H_{21}ClN_7O$, $[M+H]^+$, 398.1491; found 398.1493. R_f = 0.38 (DCM/MeOH, 5/1, v/v). Retention time: 3.91 min, 98.79 % purity.

(*S*)-(6-Chloro-4-((5-methyl-1*H*-pyrazol-3-yl)amino)quinazolin-2-yl)(2-methylpiperazin-1-yl)methanone hydrochloride (26). Light yellow solid (yield 22 %). ^{1}H NMR (400 MHz, DMSO-d_6) δ 11.50 (br, 1H), 9.83 (s, 1H), 9.46-9.44 (m, 1H), 9.02 (d, J = 1.8 Hz, 1H), 8.01 (dd, J = 1.8, 9.0 Hz, 1H), 7.92 (dd, J = 5.4, 8,8 Hz, 1H), 6.55 (d, J = 7.80 Hz, 1H), 4.88-4.86 (m, 1H), 4.52-4.49 (m, 1H), 4.17-3.78 (m, 1H), 3.54-2.91 (m, 1H), 2.32 (s, 3H), 1.45-1.37 (m, 3H). ^{13}C NMR (100 MHz, DMSO-d_6) δ 163.0, 157.3, 155.3, 145.8, 144.2, 140.9, 135.6, 132.8, 127.4, 124.1, 115.5, 98.6, 47.6, 46.4, 45.9, 42.8, 42.6, 38.8, 33.5, 16.8, 15.6, 11.3. HRMS (ESI, m/z) calcd for $C_{18}H_{21}ClN_7O$, $[M+H]^+$, 386.1491; found 386.1495. R_f = 0.34 (DCM/MeOH, 5/1, v/v). Retention time: 4.03 min, 96.24 % purity.

***(S)*-(6-Chloro-4-((5-cyclopropyl-1*H*-pyrazol-3-yl)amino)quinazolin-2-yl)(2-methylpiperazin-1-yl)methanone hydrochloride (27).** Light yellow solid (yield 26 %). ^{1}H NMR (400 MHz, DMSO-d_6) δ 11.49 (br, 1H), 9.87 (s, 1H), 9.51-9.49 (m, 1H),

9.01 (d, *J* = 1.6 Hz, 1H), 8.00 (d, *J* = 8.7 Hz, 1H), 7.91 (d, *J* = 8.9 Hz, 1H), 6.44 (d, *J* = 8.8 Hz, 1H), 4.91-4.88 (m, 1H), 4.52-4.49 (m, 1H), 4.19-3.75 (m, 1H), 3.53-3.28 (m, 2H), 3.19-2.89 (m, 3H), 2.00-1.98 (m, 1H), 1.45-1.38 (m, 3H), 1.00-0.98 (m, 2H), 0.75-0.73 (m, 2H). ^{13}C NMR (100 MHz, DMSO-d_6) δ 162.6, 156.9, 154.9, 148.0, 145.7, 135.7, 132.9, 127.2, 124.2, 115.5, 95.5, 47.7, 46.4, 45.9, 42.8, 42.6, 38.8, 33.6, 16.9, 15.6, 8.8, 7.4. HRMS (ESI, m/z) calcd for $C_{20}H_{23}ClN_7O$, $[M+H]^+$, 412.1647; found 412.1649. R_f= 0.37 (DCM/MeOH, 5/1, v/v). Retention time: 4.10 min, 100 % purity.

(*R*)-(6-Chloro-4-((5-methyl-1*H*-pyrazol-3-yl)amino)quinazolin-2-yl)(2-methylpiperazin-1-yl)methanone hydrochloride (28). Light yellow solid (yield 19 %). ^{1}H NMR (400 MHz, DMSO-d_6) δ 11.21 (br, 1H), 9.69 (br, 1H), 9.28 (br, 1H), 8.96 (s, 1H), 7.97 (dd, *J* = 1.7, 8.8 Hz, 1H), 7.87 (dd, *J* = 5.4, 8,5 Hz, 1H), 6.55 (d, *J* = 9.1 Hz, 1H), 4.90-4.87 (m, 1H), 4.52-4.49 (m, 1H), 3.74-3.45 (m, 1H), 3.36-2.89 (m, 4H), 2.30 (s, 3H),1.43-1.36 (m, 3H). ^{13}C NMR (100 MHz, DMSO-d_6) δ 163.0, 157.3, 155.4, 145.8, 144.4, 140.9, 135.6, 132.8, 127.5, 124.1, 115.5, 98.6, 47.6, 46.4, 45.9, 42.8, 42.6, 38.8, 33.5, 16.8, 15.6, 11.3. HRMS (ESI, m/z) calcd for $C_{18}H_{21}ClN_7O$, $[M+H]^+$, 386.1491; found 386.1495. R_f = 0.34 (DCM/MeOH, 5/1, v/v). Retention time: 3.99 min, 98.98 % purity.

***(R)*-(6-Chloro-4-((5-cyclopropyl-1*H*-pyrazol-3-yl)amino)quinazolin-2-yl)(2-methylpiperazin-1-yl)methanone hydrochloride (29).** Light yellow solid (yield 21 %). ^{1}H NMR (400 MHz, DMSO-d_6) δ 11.36 (br, 1H), 9.78 (s, 1H), 9.41-9.39 (m, 1H), 8.98 (s, 1H), 7.98 (d, *J* = 9.0 Hz, 1H), 7.89 (d, *J* = 8.9 Hz, 1H), 6.44 (d, *J* = 9.1 Hz,

1H), 4.93-4.86 (m, 1H), 4.52-4.48 (m, 1H), 3.76-3.45 (m, 1H), 3.35-2.87 (m, 4H), 2.02-1.98 (m, 1H), 1.44-1.37 (m, 3H), 1.00-0.98 (m, 2H), 0.74-0.73 (m, 2H). ^{13}C NMR (100 MHz, DMSO-d_6) δ 162.9, 156.9, 154.9, 147.9, 145.7, 135.7, 132.8, 127.3, 124.2, 115.5, 95.5, 47.6, 46.4, 45.9, 42.8, 42.6, 38.8, 33.6, 16.8, 15.6, 8.7, 7.4. HRMS (ESI, m/z) calcd for $C_{20}H_{23}ClN_7O$, $[M+H]^+$, 412.1647; found 412.1648. R_f = 0.38 (DCM/MeOH, 5/1, v/v). Retention time: 4.10 min, 100 % purity.

(*R*)-(6-Chloro-4-((5-methyl-1*H*-pyrazol-3-yl)amino)quinazolin-2-yl)(3-methylpiperazin-1-yl)methanone hydrochloride (30). Light yellow solid (yield 19 %). ^{1}H NMR (400 MHz, DMSO-d_6) δ 11.39 (br, 1H), 9.75-9.64 (m, 2H), 8.99 (s, 1H), 7.99 (d, J = 10.0 Hz, 1H), 7.90 (d, J = 8.8 Hz, 1H), 6.54 (d, J = 7.6 Hz, 1H), 4.47-4.43 (m, 1H), 3.92-3.83 (m, 1H), 3.54-2.98 (m, 5H), 2.31 (s, 3H), 1.36-1.12 (m, 3H). ^{13}C NMR (100 MHz, DMSO-d_6) δ 163.3, 157.3, 155.2, 145.9, 144.7, 140.8, 135.5, 132.7, 127.8, 124.0, 115.6, 98.6, 51.0, 50.5, 48.9, 44.4, 43.0, 42.6, 38.3, 15.8, 15.3, 11.4. HRMS (ESI, m/z) calcd for $C_{18}H_{21}ClN_7O$, $[M+H]^+$, 386.1491; found 386.1491. R_f = 0.34 (DCM/MeOH, 5/1, v/v). Retention time: 4.01 min, 96.53 % purity.

(*R*)-(6-Chloro-4-((5-cyclopropyl-1*H*-pyrazol-3-yl)amino)quinazolin-2-yl)(3-methylpiperazin-1-yl)methanone hydrochloride (31). Light yellow solid (yield 29 %). ^{1}H NMR (400 MHz, DMSO-d_6) δ 11.38 (br, 1H), 9.71-9.61 (m, 2H), 8.98 (s, 1H), 8.00 (d, J = 9.0 Hz, 1H), 7.90 (d, J = 8.8 Hz, 1H), 6.46 (d, J = 7.4 Hz, 1H), 4.46-4.42 (m, 1H), 3.96-3.87 (m, 1H), 3.54-2.98 (m, 5H), 2.03-1.96 (m, 1H), 1.36-1.13 (m, 3H), 1.00-0.98 (m, 2H), 0.77-0.76 (m, 2H). ^{13}C NMR (100 MHz, DMSO-d_6) δ 162.7, 157.2, 154.4, 148.1, 145.4, 135.8, 133.0, 127.2, 124.3, 115.5, 95.8, 50.9, 50.5, 48.9,

44.4, 43.0, 42.5, 42.2, 38.4, 15.7, 15.3, 8.8, 7.5. HRMS (ESI, m/z) calcd for $C_{20}H_{23}ClN_7O$, $[M+H]^+$, 412.1647; found 412.1648. R_f= 0.39 (DCM/MeOH, 5/1, v/v). Retention time: 3.92 min, 98.69 % purity.

(*S*)-(6-Chloro-4-((5-methyl-1*H*-pyrazol-3-yl)amino)quinazolin-2-yl)(3-methylpiperazin-1-yl)methanone hydrochloride (32). Light-yellow solid (yield 23 %). ^{1}H NMR (400 MHz, DMSO-d_6) δ 11.42 (br, 1H), 9.77-9.66 (m, 2H), 9.00 (s, 1H), 8.00 (d, J = 9.0 Hz, 1H), 7.91 (d, J = 8.9 Hz, 1H), 6.54 (d, J = 7.1 Hz, 1H), 4.47-4.44 (m, 1H), 3.94-3.85 (m, 1H), 3.55-2.99 (m, 5H), 2.32 (s, 3H), 1.36-1.12 (m, 3H). ^{13}C NMR (100 MHz, DMSO-d_6) δ 162.9, 157.3, 154.8, 145.6, 144.1, 141.0, 135.7, 132.9, 127.4, 124.1, 115.5, 98.7, 50.9, 50.5, 49.0, 48.9, 44.4, 43.0, 42.6, 42.2, 38.3, 15.8, 15.3, 11.4. HRMS (ESI, m/z) calcd for $C_{18}H_{21}ClN_7O$, $[M+H]^+$, 386.1491; found 386.1492. R_f= 0.34 (DCM/MeOH, 5/1, v/v). Retention time: 4.01 min, 95.35 % purity.

(*S*)-(6-Chloro-4-((5-cyclopropyl-1*H*-pyrazol-3-yl)amino)quinazolin-2-yl)(3-methylpiperazin-1-yl)methanone hydrochloride (33). Light-yellow solid (yield 22 %). ^{1}H NMR (400 MHz, DMSO-d_6) δ 11.21 (br, 1H), 9.68-9.57 (m, 2H), 8.95 (d, J = 1.8 Hz, 1H), 7.97 (dd, J = 2.0, 8.9 Hz, 1H), 7.88 (dd, J = 1.3, 8.8 Hz, 1H), 6.44 (d, J = 8.4Hz, 1H), 4.45-4.42 (m, 1H), 3.92-3.82 (m, 1H), 3.52-3.35 (m, 2H), 3.29-2.96 (m, 3H), 2.02-1.95 (m, 1H), 1.36-1.13 (m, 3H), 1.00-0.95 (m, 2H), 0.77-0.73 (m, 2H). ^{13}C NMR (100 MHz, DMSO-d_6) δ 163.5, 157.2, 155.4, 147.4, 146.0, 145.2, 135.3, 132.6, 128.1, 123.9, 115.6, 95.9, 50.9, 50.5, 48.9, 44.3, 43.0, 42.6, 42.2, 38.3, 15.7, 15.3, 8.6, 7.5. HRMS (ESI, m/z) calcd for $C_{20}H_{23}ClN_7O$, $[M+H]^+$, 412.1647; found 412.1644. R_f = 0.39 (DCM/MeOH, 5/1, v/v). Retention time: 3.89 min, 96.85 % purity.

(6-Chloro-4-((5-methyl-1*H*-pyrazol-3-yl)amino)quinazolin-2-yl)(3,5-dimethylpiperazin-1-yl)methanone hydrochloride (34). Light-yellow solid (yield 17 %). ^{1}H NMR (400 MHz, DMSO-d_6) δ 11.35 (br, 1H), 9.83 (d, J = 9.3 Hz, 1H), 9.45-9.47 (m, 1H), 8.98 (d, J = 1.8 Hz, 1H), 7.99 (dd, J = 2.0, 8.9 Hz, 1H), 7.89 (d, J = 8.9 Hz, 1H), 6.52 (s, 1H), 4.60 (d, J = 12.8 Hz, 1H), 3.94 (d, J = 12.6 Hz, 1H), 3.36-3.30 (m, 2H), 3.19 (t, J = 13.5 Hz, 1H), 3.00 (t, J = 12.2 Hz, 1H), 2.32 (s, 1H), 1.36 (d, J = 6.4 Hz, 3H), 1.13 (d, J = 6.2 Hz, 3H). ^{13}C NMR (100 MHz, DMSO-d_6) δ 163.0, 157.3, 155.1, 145.9, 144.4, 140.7, 135.5, 132.7, 127.5, 124.0, 115.6, 98.6, 51.8, 51.2, 48.5, 44.0, 15.9, 15.4, 11.4. HRMS (ESI, m/z) calcd for $C_{19}H_{23}ClN_7O$, $[M+H]^+$, 400.1647; found 400.1650. R_f = 0.44 (DCM/MeOH, 5/1, v/v). Retention time: 4.03 min, 96.78 % purity.

(6-Chloro-4-((5-cyclopropyl-1*H*-pyrazol-3-yl)amino)quinazolin-2-yl)(3,5-dimethylpiperazin-1-yl)methanone hydrochloride (35). Light-yellow solid (yield 25 %). ^{1}H NMR (400 MHz, DMSO-d_6) δ 11.20 (br, 1H), 9.72 (d, J = 9.8 Hz, 1H), 9.45-9.40 (m, 1H), 8.96 (d, J = 1.7 Hz, 1H), 7.98 (dd, J = 2.0, 8.9 Hz, 1H), 7.88 (d, J = 8.9 Hz, 1H), 6.44 (s, 1H), 4.63-4.60 (m, 1H), 4.03 (q, J = 7.1 Hz, 1H), 3.95 (d, J = 13.3 Hz, 1H), 3.36-3.29 (m, 2H), 3.19 (t, J = 13.5 Hz, 1H), 2.97 (t, J = 13.4 Hz, 1H), 2.02-1.96 (m, 1H), 1.36 (d, J = 6.4 Hz, 3H), 1.14 (d, J = 6.2 Hz, 3H), 1.01-0.96 (m, 2H), 0.78-0.74 (m, 2H). ^{13}C NMR (100 MHz, DMSO-d_6) δ 162.6, 157.2, 154.7, 147.8, 145.6, 143.9, 135.7, 132.9, 127.3, 124.0, 115.5, 95.9, 51.8, 51.2, 48.5, 44.1, 15.9, 15.4, 8.6, 7.5. HRMS (ESI, m/z) calcd for $C_{21}H_{25}ClN_7$, $[M+H]^+$, 426.1804; found

426.1800. R_f = 0.37 (DCM/MeOH, 5/1, v/v). Retention time: 4.10 min, 96.76 % purity.

(*R*)-(6-Chloro-4-((5-cyclopropyl-1*H*-pyrazol-3-yl)amino)quinazolin-2-yl)(3-ethyl piperazin-1-yl)methanone hydrochloride (36). Light-yellow solid (yield 19 %). ^{1}H NMR (400 MHz, DMSO-d_6) δ 11.55 (br, 1H), 9.80-9.75 (m, 2H), 9.02 (s, 1H), 8.01 (dd, J = 1.8, 9.0 Hz, 1H), 7.92 (dd, J = 5.6, 8.8 Hz, 1H), 6.47 (d, J = 10.4 Hz, 1H), 4.45 (d, J = 11.0 Hz, 1H), 4.03-3.90 (m, 1H), 3.60-3.01 (m, 5H), 2.03-1.99 (m, 1H), 1.81-1.69 (m, 1H), 1.66-1.44 (m, 1H), 1.05-0.69 (m, 7H). ^{13}C NMR (100 MHz, DMSO-d_6) δ 162.8, 157.0, 154.7, 147.9, 145.6, 144.2, 135.7, 132.9, 127.5, 124.1, 115.6, 95.8, 56.3, 55.6, 47.5, 43.3, 42.8, 42.6, 38.7, 23.1, 22.8, 10.1, 9.6, 8.7, 7.5. HRMS (ESI, m/z) calcd for $C_{21}H_{25}ClN_7$, $[M+H]^+$, 426.1804; found 426.1801. R_f = 0.39 (DCM/MeOH, 5/1, v/v). Retention time: 4.11 min, 95.17 % purity.

(*R*)-(4-((5-Cyclopropyl-1*H*-pyrazol-3-yl)amino)quinazolin-2-yl)(3-methylpipera zin-1-yl)methanone hydrochloride (37). Yellow solid (yield 23 %). ^{1}H NMR (400 MHz, DMSO-d_6) δ 12.04 (br, 1H), 9.92 (s, 2H), 8.90 (d, J = 8.3 Hz, 1H), 8.07 (t, J = 7.8 Hz, 1H), 8.00 (d, J = 8.4 Hz, 1H), 7.81 (t, J = 6.9 Hz, 1H), 6.43 (d, J = 4.6 Hz, 1H), 4.49-4.43 (m, 1H), 4.20-4.12 (m, 1H), 3.66-3.10 (m, 5H), 2.06-1.99 (m, 1H), 1.38-1.16 (m, 3H), 1.01-0.99 (m, 2H), 0.79-0.78 (m, 2H). ^{13}C NMR (100 MHz, DMSO-d_6) δ 161.2, 158.2, 152.6, 147.8, 145.4, 136.5, 129.4, 125.2, 114.0, 96.4, 50.9, 50.4, 48.9, 44.7, 43.1, 42.5, 42.2, 38.7, 15.7, 15.3, 8.7, 7.4. HRMS (ESI, m/z) calcd for $C_{20}H_{24}N_7O$, $[M+H]^+$, 378.2037; found 378.2039. R_f = 0.19 (DCM/MeOH, 5/1, v/v). Retention time: 4.05 min, 95.06 % purity.

(*R*)-(7-Chloro-4-((5-cyclopropyl-1*H*-pyrazol-3-yl)amino)quinazolin-2-yl)(3-methylpiperazin-1-yl)methanone hydrochloride (38). Off-white solid (yield 24 %). ^{1}H NMR (400 MHz, DMSO-d_6) δ 11.70 (br, 1H), 9.86 (s, 2H), 8.88 (dd, J = 2.4, 9.0 Hz, 1H), 7.99 (s, 1H), 7.81 (dt, J = 2.1, 8.9 Hz, 1H), 6.44 (d, J = 5.4 Hz, 1H), 4.45-4.42 (m, 1H), 4.01-3.92 (m, 1H), 3.59-3.29 (m, 3H), 3.25-3.01 (m, 2H), 2.05-1.99 (m, 1H), 1.37-1.15 (m, 3H), 1.01-0.99 (m, 2H), 0.78-0.77 (m, 2H). ^{13}C NMR (100 MHz, DMSO-d_6) δ 162.4, 157.6, 154.7, 148.4, 145.1, 140.3, 129.2, 127.2, 124.1, 123.9, 113.3, 95.8, 50.9, 50.4, 48.9, 44.5, 43.0, 42.6, 42.2, 38.4, 15.7, 15.3, 8.9, 7.4. HRMS (ESI, m/z) calcd for $C_{20}H_{23}ClN_7O$, $[M+H]^+$, 412.1647; found 412.1645. R_f = 0.19 (DCM/MeOH, 5/1, v/v). Retention time: 4.10 min, 99.63 % purity.

(*R*)-(4-((5-Cyclopropyl-1*H*-pyrazol-3-yl)amino)-6-fluoroquinazolin-2-yl)(3-methylpiperazin-1-yl)methanone hydrochloride (39). Light yellow solid (yield 13 %). ^{1}H NMR (400 MHz, DMSO-d_6) δ 11.63 (br, 1H), 9.89 (s, 2H), 8.80 (d, J = 9.9 Hz, 1H), 8.02 (dd, J = 5.4, 9.2 Hz, 1H), 7.93 (t, J = 8.3 Hz, 1H), 6.46 (d, J = 5.6 Hz, 1H), 4.46-4.43 (m, 1H), 4.02-3.93 (m, 1H), 3.60-3.29 (m, 3H), 3.27-3.01 (m, 2H), 2.05-2.01 (m, 1H), 1.38-1.15 (m, 3H), 1.01-0.99 (m, 2H), 0.80-0.76 (m, 2H). ^{13}C NMR (100 MHz, DMSO-d_6) δ 161.2, 158.2, 152.6, 147.8, 145.4, 136.5, 129.4, 125.2, 114.0, 96.4, 50.9, 50.4, 48.9, 44.7, 43.1, 42.5, 42.2, 38.7, 15.7, 15.3, 8.7, 7.4. HRMS (ESI, m/z) calcd for $C_{20}H_{23}FN_7O$, $[M+H]^+$, 396.1943; found 396.1944. R_f = 0.22 (DCM/MeOH, 5/1, v/v). Retention time: 4.00 min, 96.25 % purity.

(*R*)-(6-Bromo-4-((5-cyclopropyl-1*H*-pyrazol-3-yl)amino)quinazolin-2-yl)(3-methylpiperazin-1-yl)methanone hydrochloride (40). Light yellow solid (yield 15 %).

^{1}H NMR (400 MHz, DMSO-d_6) δ 11.46 (br, 1H), 9.78-9.70 (m, 2H), 9.14 (s, 1H), 8.11 (d, J = 9.0, Hz, 1H), 7.84 (d, J = 8.8 Hz, 1H), 6.44 (d, J = 6.7 Hz, 1H), 4.46-4.42 (m, 1H), 3.96-3.88 (m, 1H), 3.56-3.28 (m, 3H), 3.26-2.99 (m, 2H), 2.04-1.97 (m, 1H), 1.37-1.14 (m, 3H), 1.00-0.98 (m, 2H), 0.78-0.76 (m, 2H). ^{13}C NMR (100 MHz, DMSO-d_6) δ 162.5, 159.1, 157.0, 154.5, 147.9, 145.6, 138.4, 127.3, 121.3, 115.9, 95.9, 50.9, 50.4, 48.9, 44.5, 43.0, 42.6, 42.2, 38.4, 15.7, 15.3, 8.7, 7.4. HRMS (ESI, m/z) calcd for $C_{20}H_{23}BrN_7O$, $[M+H]^+$, 458.1122; found 458.1123. R_f = 0.22 (DCM/MeOH, 5/1, v/v). Retention time: 4.10 min, 96.75 % purity.

(*R*)-(4-((5-Cyclopropyl-1*H*-pyrazol-3-yl)amino)-6-methoxyquinazolin-2-yl)(3-methylpiperazin-1-yl)methanone hydrochloride (41). Light yellow solid (yield 21 %). ^{1}H NMR (400 MHz, DMSO-d_6) δ 12.01 (br, 1H), 9.85-9.82 (m, 2H), 8.40 (d, J = 2.0 Hz, 1H), 7.95 (d, J = 9.1 Hz, 1H), 7.70 (d, J = 9.1 Hz, 1H), 6.47 (d, J = 4.0 Hz, 1H), 4.50-4.43 (m, 1H), 4.27-4.20 (m, 1H), 3.99 (s, 3H), 3.66-3.33 (m, 3H), 3.27-3.06 (m, 2H), 2.05-1.99 (m, 1H), 1.38-1.15 (m, 3H), 1.01-0.99 (m, 2H), 0.79-0.78 (m, 2H). ^{13}C NMR (100 MHz, DMSO-d_6) δ 161.3, 159.9, 156. 8, 149.9, 147.6, 146.0, 127.5, 125.4, 115.3, 105.0, 96.0, 57.3, 50.9, 50.4, 49.1, 45.0, 43.3, 42.5, 42.2, 38.9, 15.7, 15.3, 8.7, 7.4. HRMS (ESI, m/z) calcd for $C_{21}H_{26}N_7O_2$, $[M+H]^+$, 408.2142; found 408.2145. R_f = 0.19 (DCM/MeOH, 5/1, v/v). Retention time: 4.02 min, 96.12 % purity.

1-Methyl-4-nitro-1*H*-imidazole (43). To a solution of 4-nitro-1*H*-imidazole (**42**, 446 mg, 4.0 mmol) in CH_3CN (20 mL) was added K_2CO_3 (828 mg, 7.0 mmol) and CH_3I (0.44 mL, 4.8 mmol). The mixture was stirred at 65 ℃ for 12 h. After cooling to room temperature (rt), diethylamine (20 mL) was added to quench the reaction. The

reaction mixture was filtered. The filtrate was concentrated and purified by chromatography (20 % EtOAc/hexanes) to afford **43** (361 mg, 72 % yield) as an off-white solid. ^{1}H NMR (400 MHz, $CDCl_3$) δ 7.78 (d, J = 1.4 Hz, 1H), 3.43 (s, 3H). MS (ESI) m/z :127.7 $[M+H]^+$, 149.7 $[M+Na]^+$. R_f = 0.47 (DCM/MeOH, 20/1, v/v).

1-Methyl-1*H*-imidazol-4-amine hydrochloride (44a). To a solution of 1-methyl-4-nitro-1*H*-imidazole (**43**, 267 mg, 2.1 mmol) in MeOH (20 mL) was added 10 % wt Pd/C (40 mg). The reaction mixture was hydrogenated under hydrogen (1 atm) for 8 h. The Pd/C was removed by filtration, and the filtrate was concentrated to yield 1-methyl-1*H*-imidazol-4-amine, which was dissolved in EtOH (10 mL) and cooled to 0 °C. A saturated solution of HCl in ethanol (4 mL) was added, and the reaction was stirred at 0 °C for 1 h. The solid was filtered and washed with ethanol to provide **44a** (179 mg, 64 % yield) as an off-white solid. ^{1}H NMR (400 MHz, DMSO-d_6) δ 8.37 (d, J = 1.2 Hz, 1H), 7.81 (d, J = 0.7 Hz, 1H), 3.76 (s, 3H).

Compound **44b-d** were prepared in a similar manner as compound **44a**, using **47a**, **45** and **47b**, respectively instead of **43**.

1-Isopropyl-4-nitro-1*H*-imidazole (45). To a solution of 4-nitro-1*H*-imidazole (**42**, 226 mg, 2.0 mmol) in anhydrous DMF (10 mL) was added K_2CO_3 (552 mg, 4.0 mmol) and 2-bromopropane (0.19 mL, 2.4 mmol). The mixture was stirred at 65°C overnight. The reaction mixture was filtered, and the filtrate was concentrated and purified by chromatography (20 % EtOAc/hexanes) to afford **45** as an off-white solid (239 mg, 77 % yield).

1,4-Dinitro-1*H*-imidazole (46). To a suspension of 4-nitro-1*H*-imidazole (**42**, 500 mg, 4.4 mmol) in AcOH (9 mL) was added HNO_3 (2.2 mL) and Ac_2O (6 mL) at 0 °C. The reaction mixture was stirred at ambient temperature (< 25°C) for 1 h and poured onto ice (50 g). The reaction solution was then extracted with ethyl acetate (3×15 mL). The combined organic extracts were washed with water (3×15 mL) and 1 M $NaHCO_3$ (3×15 mL), dried over $MgSO_4$, filtered and concentrated to yield **46** as an off-white solid (630 mg, 91 % yield). ^{1}H NMR (400 MHz, $CDCl_3$) δ 8.54 (d, J = 1.6 Hz, 1H), 8.40 (d, J = 1.6 Hz, 1H). R_f = 0.70 (DCM/MeOH, 20/1, v/v).

1-Cyclopropyl-4-nitro-1*H*-imidazole (47a). Together, 1,4-dinitro-1*H*-imidazole (**46**, 630 mg, 4.0 mmol) and cyclopropanamine (0.30 mL, 4.4 mmol) were dissolved in water (12 mL) and MeOH (12 mL). The reaction mixture was stirred at rt for 24 h and diluted with water (30 mL). The reaction mixture was extracted with ethyl acetate (4×15 mL). The organic layers were dried over Na_2SO_4 and concentrated to afford **47a** as a white solid (390 mg, 64 % yield). ^{1}H NMR (400 MHz, $CDCl_3$) δ 7.76 (s, 1H), 7.47 (s, 1H), 3.45-3.40 (m, 1H), 1.12-0.99 (m, 4H).

2,6-Dichloro-*N*-(1-methyl-1*H*-imidazol-4-yl)quinazolin-4-amine (51a). To a solution of **50** (465 mg, 2.0 mmol) in 5 mL of anhydrous DMF was added 1-methyl-1*H*-imidazol-4-amine hydrochloride (**44a**, 267 mg, 2.0 mmol) and DIEA (0.39 mL, 2.4 mmol) at 0 °C. The reaction was stirred at 0 °C for 3 h and poured into water (50 mL). The solid was filtered and dried to provide the title compound (423 mg, 72 % yield) as a light-yellow solid. ^{1}H NMR (400 MHz, DMSO-d_6) δ 11.08 (s, 1H), 8.94 (d, J = 2.2 Hz, 1H), 7.85 (dd, J = 2.2, 8.9 Hz, 1H), 7.70 (d, J = 8.9, 1H),

7.56 (d, J = 1.0 Hz, 1H), 7.55 (d, J = 1.4 Hz, 1H), 3.73 (s, 3H). R_f = 0.22 (DCM/MeOH, 20/1, v/v). MS (ESI) m/z 291.9 $(M-H)^-$.

Tert-butyl (1-(6-chloro-4-((1-methyl-1*H*-imidazol-4-yl)amino)quinazolin-2-yl)piperidin-4-yl) carbamate (52a). A reaction tube was charged with 2,6-dichloro-*N*-(1-methyl-1*H*-imidazol-4-yl)quinazolin-4-amine (**51a**, 196 mg, 0.67 mmol), *tert*-butyl piperidin-4-ylcarbamate (268 mg, 1.34 mmol), hydrochloric acid (HCl, 10 μL) and 5 mL of ethanol. The tube was sealed, and the mixture was heated at 120 °C for 15 h. After cooling, the reaction was concentrated and purified by silica gel chromatography (2 % MeOH/DCM) to provide the title compound (221 mg, 72 % yield) as a white solid. ^{1}H NMR (400 MHz, DMSO-d_6) δ 10.20 (s, 1H), 8.62 (d, J = 2.1Hz, 1H), 7.53-7.51 (m, 2H), 7.33 (s, 1H), 7.30 (d, J = 8.9 Hz, 1H), 6.85 (d, J = 7.8 Hz, 1H), 4.67-4.64 (m, 2H), 3.70 (s, 3H), 3.57-3.54 (m, 1H), 3.04 (t, J = 11.7 Hz, 2H), 1.84-1.82 (m, 2H), 1.39 (s, 9H), 1.32-1.23 (m, 2H). R_f = 0.25 (DCM/MeOH, 20/1, v/v). MS (ESI) m/z 458.3 $(M+H)^+$.

2-Amino-5-chlorobenzamide (56). A mixture of 2-amino-5-chlorobenzoic acid (**48**, 5.0 g, 29.1 mmol) and bis(trichloromethyl) carbonate (2.9 g, 9.9 mmol) in 50 mL of anhydrous THF was refluxed for 16 h. After cooling, the THF was removed with a vacuum. The reaction mixture was diluted with 233 mL of 1N NH_3-H_2O solution. After stirring for 1 h at 65 °C, the reaction mixture was cooled to 0 °C and the precipitated solid was collected *via* filtration to provide **56** (4.23 g, 85 % yield) as a white solid. After a high-vacuum dry, the product was used directly for the next step.

^{1}H NMR (400 MHz, DMSO-d_6) δ 7.84 (s, 1H), 7.59 (d, J = 2.5 Hz, 1H), 7.19 (s, 1H), 7.15 (dd, J = 2.5, 8.8 Hz, 1H), 6.71 (d, J = 8.8 Hz, 1H), 6.39 (br, 2H). R_f = 0.38 (DCM/MeOH, 30/1, v/v, 0.5 % CH_3COOH). mp 169-170 °C. MS (ESI) m/z 168.8 $(M-H)^-$.

Ethyl 2-((2-carbamoyl-4-chlorophenyl)amino)-2-oxoacetate (57). To a solution of 2-amino-5-chlorobenzamide (**56**, 3.0 g, 17.6 mmol) and triethylamine (2.9 mL, 21.1 mmol) in 110 mL of anhydrous THF was added ethyl 2-chloro-2-oxoacetate (2.1 mL, 19.4 mmol) at 0 °C. The reaction mixture was stirred at rt for 3 h and diluted with water (300 mL). The solid was filtered and washed with water to provide **57** (4.46 g, 94 % yield) as a white solid. ^{1}H NMR (400 MHz, DMSO-d_6) δ 13.02 (s, 1H), 8.56 (d, J = 2.5, 1H), 8.47 (s, 1H), 7.80 (s, 1H), 7.97 (d, J = 2.4, 1H), 7.66 (dd, J = 2.4, 9.0 Hz, 1H), 4.31 (q, J = 7.1, 1H), 1.32 (t, J = 7.1, 1H). R_f = 0.41 (DCM/MeOH, 30/1, v/v, 0.5 % CH_3COOH). mp 201-202 °C. MS (ESI) m/z 293.0 $(M+Na)^+$.

Ethyl 6-chloro-4-oxo-3,4-dihydroquinazoline-2-carboxylate (58). To a solution of ethyl 2-((2-carbamoyl-4-chlorophenyl)amino)-2-oxoacetate (**57**, 2.70 g, 10.0 mmol) in ethanol (54 mL) was added an ethanol solution (8.2 mL) of sodium ethanolate (0.82 g, 12.0 mmol) at 0 °C. The reaction mixture was stirred at 0 °C for 3 h and was acidified to pH=3-4 with a 2 N HCl solution. The solid was filtered and washed with water to provide **58** (2.17 g, 86 % yield) as a white solid. ^{1}H NMR (400 MHz, DMSO-d_6) δ 12.83 (s, 1H), 8.10 (d, J = 2.4 Hz, 1H), 7.92 (dd, J = 2.4, 8.7 Hz, 1H), 7.85 (d, J = 8.7 Hz, 1H), 4.39 (q, J = 7.1 Hz, 2H), 1.35 (t, J = 7.1 Hz, 3H). R_f = 0.62

(DCM/MeOH, 30/1, v/v, 0.5 % CH_3COOH). m.p 267-268 °C. MS (ESI) m/z 275.1$(M+Na)^+$, 250.8 $(M-H)^-$.

6-Chloro-4-oxo-3,4-dihydroquinazoline-2-carboxylic acid (59). To a solution of ethyl 6-chloro-4-hydroxyquinazoline-2-carboxylate (**58**, 6.0 g, 23.8 mmol) in ethanol (80 mL) and water (80 mL) was added NaOH (7.8 g, 195 mmol). The reaction mixture was stirred at 78 °C in an oil bath for 1 h. After cooling, the reaction mixture was acidified to pH=2 with a 2 N HCl solution. The solid was filtered and washed with water to provide **59** (5.11 g, 96 % yield) as a white solid. ^{1}H NMR (400 MHz, DMSO-d_6) δ 7.90 (s, 1H), 7.69 (d, J = 9.1 Hz, 1H), 7.55 (s, 1H). R_f = 0.30 (DCM/MeOH, 30/1, v/v, 0.5 % CH_3COOH). MS (ESI) m/z 222.8 $(M-H)^-$. mp 242 °C.

4,6-Dichloroquinazoline-2-carbonyl chloride (60). Sulfurous dichloride (0.77 mL, 10.7 mmol) was added to a solution of 6-chloro-4-hydroxyquinazoline-2-carboxylic acid (**59**, 200 mg, 0.89 mmol) and DMF (2 drop) in chloroform (4 mL). The reaction mixture was reflux for 3 h. After the completion of the reaction as indicated by TLC, the reaction mixture was evaporated in *vacuo* to obtain a light-yellow solid (**60**, 233 mg, quantitative yield) which was used for the next step without further purification.

***Tert*-butyl 4-(4,6-dichloroquinazoline-2-carbonyl)piperazine-1-carboxylate (65a).** To a solution of freshly prepared 4,6-dichloroquinazoline-2-carbonyl chloride (**60**, 233 mg, 0.89 mmol) and triethylamine (0.37 mL, 2.67 mmol) in anhydrous dichloromethane (10 mL) was added *tert*-butyl piperazine-1-carboxylate (166 mg, 0.89 mmol) at -35 °C. The resulting solution was stirred at -35 °C for 0.5 h and quenched with water (10 mL). The reaction mixture was extracted with

dichloromethane (3×15 mL). The combined organic extracts were collected, dried, and concentrated under reduced pressure to provide a crude mixture, which was purified by silica gel chromatography (2 % MeOH/DCM) to provide the title compound (238 mg, 65 % yield) as a white solid. ^{1}H NMR (400 MHz, DMSO-d_6) δ 8.32 (d, J = 2.1 Hz, 1H), 8.08 (d, J = 9.0 Hz, 1H), 7.97 (dd, J = 2.3, 9.0 Hz, 1H), 3.85 (t, J = 4.9 Hz, 2H), 3.61 (t, J = 5.4 Hz, 2H), 3.53-3.51 (m, 2H), 3.45-3.42 (m, 2H), 1.49 (s, 9H). mp 301 °C.

***Tert*-butyl 4-(6-chloro-4-((5-methyl-1*H*-pyrazol-3-yl)amino)quinazoline-2-carbonyl)piperazine-1- carboxylate (66a).** To a solution of *tert*-butyl 4-(4,6-dichloroquinazoline-2-carbonyl)piperazine-1-carboxylate (**65a**, 145 mg, 0.35 mmol), KI (67.4 mg, 0.41 mmol), and DIEA (0.08 mL, 0.45 mmol) in 5 mL of anhydrous DMF was added 5-methyl-1*H*-pyrazol-3-amine (36.9 mg, 0.38 mmol). The resulting solution was stirred at 65°C for 8 h and diluted with water (50 mL). The precipitated solid was collected *via* filtration and purified by silica gel chromatography (2 % MeOH/DCM) to provide the title compound (105 mg, 63 % yield) as an off-white solid. ^{1}H NMR (400 MHz, DMSO-d_6) δ 12.28 (s, 1H), 10.71 (s, 1H), 8.89 (s, 1H), 7.89 (dd, J = 2.0, 8.9 Hz, 1H), 7.80 (d, J = 8.9 Hz, 1H), 6.57 (s, 1H), 3.65-3.62 (m, 2H), 3.49-3.40 (m, 2H), 3.29-3.28 (m, 4H), 2.27 (s, 3H), 1.41 (s, 9H). mp 290 °C.

PAK4 Expression, Purification, and Crystallization. The cDNA encoding the kinase domain (resides 300 to 591) of human PAK4 was cloned into a modified

pET28b vector with an *N*-terminal 10xHis tag followed by a SUMO tag. The recombinant protein was overexpressed in *E. coli* BL21 (DE3). After overnight induction with 0.2 mM isopropyl *β*-D-thiogalactoside (IPTG) at 16 ℃ in LB medium, the cells were harvested and suspended in buffer (300 mM NaCl, 20 mM Tris, pH 7.5). Then, the cells were lysed with an Emulsiflex C3 (Avestin) high-pressure homogenizer. After centrifugation at ×32,000 g, the supernatant was applied to a HisTrap column (GE Healthcare) and subjected to ion-exchange chromatography (HiTrap Q HP). Then, the resultant protein was digested overnight by ULP1 protease. The post-cleavage mixture was purified with a fresh HisTrap column to remove His-SUMO tags and further purified using a Superdex 200 gel-filtration column (GE Healthcare). The purified protein was concentrated to 8 mg/mL and stored at -80 ℃ for future use.

The PAK4 kinase domain and inhibitors **10a**, **30**, **31** were mixed at a molar ratio of 1:2. After incubation at 4 ℃ for 1 h, crystallization screens were performed using an Art Robbins Gryphon crystallization robot by mixing equal volumes of PAK4-inhibitor complex with different screening conditions from commercial crystallization kits. Crystals were obtained under the following buffer conditions: 25% PEG3350, 0.1 M HepesNa, pH 7.5 for the **10a** complex; 1.0 M sodium acetate trihydrate, 0.1 M imidazole, pH 6.5 for the **30** complex; and 0.5 M magnesium formate dehydrate, 0.1 M HepesNa, pH 7.5 for the **31** complex, respectively.

Data collection and structure determination. The crystals were briefly soaked in a cryo-protectant composed of reservoir solution supplemented with 20% ethylene

glycol and flash frozen in liquid nitrogen for data collection at 100 K. Data collection was performed at beamline BL17U1 at the Shanghai Synchrotron Radiation Facility. The diffraction data were indexed, integrated and merged using the HKL2000 software package (http://www.hkl-xray.com). The structures were solved using the molecular replacement method with the published PAK4 kinase domain structure (PDB code 2J0I) as a search model. Structure refinement was performed using PHENIX,[42] and iterative manual model building was performed using COOT.[43]

The PAK1 and PAK4 Biochemical Assay to Measure the K_i. In a polypropylene plate, PAK1 (kinase domain) and PAK4 (kinase domain), peptide substrate (Ser/Thr19, Ser/Thr20) labeled with both coumarin (donor fluorophore) and fluorescein (acceptor fluorophore), ATP (K_m), and the test compound were incubated together in kinase reaction buffer. The 10 μL assay mixtures contained 50 mM HEPES (pH 7.5), 0.01 % Brij-35, 10 mM $MgCl_2$, 1 mM EGTA, 2 μM FRET peptide substrate, and PAK enzyme (20 pM PAK1 KD; 80 pM PAK4 KD). In all cases, each PAK biochemical assay used ATP at a final concentration equal to its $K_{m\ apparent}$. Incubations were carried out at 22 °C. Prior to the assay, the enzyme, FRET peptide substrate and serially diluted test compounds were pre-incubated together in assay buffer (7.5 μL) for 15 minutes, and the assay was initiated by the addition of 2.5 μL assay buffer containing 4x the final ATP concentration (these are the 4x concentrations: 160 μM PAK1 and 16 μM PAK4). Following a 60-minute incubation, the assay mixtures were quenched by the addition of 5 μL of Z'-Lyte development reagent, and 1 hour later, the emissions of Coumarin (445 nm) and Fluorescein (520

nm) were determined after excitation at 400 nm using an EnVision plate reader (Perkin Elmer). The high ratio of coumarin/fluorescein represents a 0 % phosphorylation rate, while a low ratio of coumarin/fluorescein represents 100 % phosphorylation rate. The curves were fit by XLfit5 as % inhibition vs. log [compound concentration] using a 4-parameter logistic model, model 205. The K_i values reported in this manuscript were calculated by converting the IC_{50} value (generated using a non-linear least squares fit of the concentration-response data to a four-parameter equation) to the K_i value by employing the Cheng-Prusoff equation with the XLFIT5 software.[44]

The Truncated PAK4 Kinase Expression. The truncated PAK4 kinase domain was expressed and purified as reported earlier[45]. The purified protein was subsequently used for biophysical assay, DSF and SPR.

Differential Scanning Fluorimetry (DSF). DSF screening experiments were carried out using a QuantStudio™ 6 Flex Real-time PCR System (Applied Biosystems). The detection filter was chosen for SYPRO Orange ($\lambda_{excitation}$ = 550 ± 11 nm, $\lambda_{emission}$ = 586 ± 10 nm), and the scanning temperature was set from 25 °C to 90 °C at a ramp rate of 0.5 °C/min.

The truncated PAK4 protein was diluted to 0.1 mg/mL (2.7 μM) in HEPES buffer (50 mM HEPES, 150 mM NaCl, 0.02% P20, 1 mM ATP, and 5 mM $MgCl_2$) containing (10×) SYPRO Orange (Thermo Fisher Scientific). The diluted protein solution was added to a 96-well clear PCP plates (Bio-Rad) on ice, with 25 μL of the solution per well. The inhibitor compounds were dissolved in DMSO at a concentration of 10 mM

as a stock solution. Prior to use, the stock solutions were diluted to 1 mM in DMSO, and 0.5 μL (2% v/v) of the compound solution dropped to each well for DSF assay. Final concentration of the PAK4 protein is 2.7 μM, and concentration of compound is 20 μM. DMSO was used as the reference solvent. After sealing with Optical Adhesive Film, the plate was gently vortexed, centrifuged, and analyzed in the Real-time PCR System. The heating cycle included 2 mins pre-warming step at 25 °C, and subsequent gradient between 25 °C and 90 °C, each of 0.5 °C ramp.

All of reactions were performed in triplicate. Analysis of the data was primarily performed by ocular inspection of individual curves, and fitting T_m to sigmoidal transitions, where applicable, was performed using an Excel script.

Surface Plasmon Resonance (SPR). SPR biosensing experiments were performed using a four-channel Biacore T200 instrument (GE Healthcare, Sweden). Streptavidin-functionalized sensor chips (Series S SA chip, GE Healthcare) were chosen for PAK4 immobilization *via* a biotin-streptavidin capture-coupling protocol. HBS-N buffer (10 mM HEPES, 150 mM NaCl, pH 7.4, GE Healthcare) supplemented with 5 mM $MgCl_2$ was used as running buffer for the protein immobilization. All binding experiments were conducted in HBS-N buffer supplemented with 5 mM $MgCl_2$, and 0~5% of DMSO at 22 ^oC.

Briefly, the truncated biotin-PAK4 (20 μg/mL) diluted in the immobilization buffer was introduced onto a streptavidin sensor chip with a flow rate of 10 μL/min, and a response target set at 2,000 RU. This procedure led to a site-specific (C-terminal), stable and robust PAK4 layer of 1,800 ~ 2,200 RU, which was used for ligands-kinase

protein interaction analysis. For the kinetic binding analysis, the T200 standard method LMW kinetic was chosen. The contact time was set at 60 s and dissociation time of 120~300 s at a flow rate of 30 μL/min. Data processing and analysis was performed using Biacore T200 evaluation software (GE Healthcare). Prior to the kinetic fitting, double referencing was applied by subtracting a reference signal and a blank injection signal.

Cell Viability Assays. The viability of cells was determined using the MTT assay method as previously described.[24]

Wound Healing Assay. For the wound healing assay, A549 cells were cultured to confluence in 6-well plates and wounded using a sterilized pipet tip to make a straight scratch. The wounded cell monolayers were washed three times with phosphate-buffered saline (PBS) and incubated in serum free medium. Then cells were treated with compound **31** with different concentrations followed by a 48 h incubation and photographed at 24 and 48 h with an inverted microscope (AX-70; Olympus).

Cell Migration and Invasion Assays. Migration and invasion assays were performed using modified Boyden chambers with a polycarbonate nucleopore membrane, as previously described.[24]

Western Blot Analysis. To determine the expression levels of proteins, whole cell extracts were prepared from 1×10^6 cells in RIPA lysis buffer (50 mM Tris HCl at pH 7.4, 150 mM NaCl, 1 % Nonidet P-40, 0.25 % Na-deoxycholate, 1 mM EDTA and a protease inhibitor cocktail). Equal amounts of denatured protein were separated by

SDS-PAGE and transferred to a PVDF membrane (Millipore). The membrane was blocked with 5 % nonfat dry milk in TBS-T (20 mM Tris at pH 7.4, 137 mM NaCl, and 0.05 % Tween-20) for 3 h at room temperature, and the proteins were probed with antibodies specific to phospho-cofilin, cofilin, LIMK1, phospho-LIMK1, PAK4, phospho-PAK4/Ser474, phospho-GEF-H1, GEF-H1 and MMP-2. All PVDF membranes were detected by chemiluminescence (ECL, Pierce Technology). To assure equal loading, membranes were stripped and re-probed with antibody against GAPDH (Shang Hai Kangchen).

Liver Microsomal Stability Assay. These measurements were performed as previously described[46]. Two parallel determinations in microsomes, with and without the NADPH regenerating system were performed for selected compounds. Briefly, the compounds were preincubated with microsomes (human microsome, BD Gentest, lot No. 38292; rat microsome, Xenotech, Lot No. 1310030) (0.5 mg/mL) at 1 μM for 10 min at 37°C in potassium phosphate buffer (100 mM at pH 7.4 with 10 mM $MgCl_2$). The reactions were initiated by adding prewarmed cofactors (1 mmol NADPH). After incubation for different times (0, 5, 10, 20, 30, and 60 min) at 37 °C, cold acetonitrile was added to precipitate the protein. Then, the samples were centrifuged, and the supernatants were analyzed by LC/MS/MS.

Stability Assay in Rat Blood Plasma. Compound **31** was incubated in a concentration of 2 μM in SD rat blood plasma (BioreclamationIVT, batch No. RAT303151) at 37 °C. Samples were taken at the indicated time points during the incubation (0, 10, 30, 60 and 120 min in duplicate). The reactions terminated with the

addition of 400 μL of cold stop solution (200 ng/mL tolbutamide and 200 ng/mL labetalol in 50 % MeOH/acetonitrile). The plates were centrifuged (4,000 rpm for 10 min), and the supernatants were analyzed by LC/MS/MS.

Cytochrome P450 Inhibition Assay. Cytochrome P450 inhibition was evaluated in human liver microsomes (0.25 mg/mL) using five specific probe substrates (CYP1A2, 10 μM phenacetin; CYP2C9, 5 μM diclofenac; CYP2C19, 30 μM *S*-mephenytoin; CYP2D6, 5 μM dextromethorphan; and CYP3A4, 2 μM midazolam) in the presence of multiple concentrations of the test compound (0.05-50 μM). After pre-incubation at 37 °C for 10 min, the reaction was initiated by the addition of 20 μL NADPH to a final concentration of 10 mM. The mixture was incubated at 37 °C for 10 min and the reaction was terminated by the addition of 400 μL of cold stop solution (200 ng/mL tolbutamide and 200 ng/mL labetalol in acetonitrile). After the reactions were terminated, the plates were centrifuged, and the supernatants were analyzed by LC/MS/MS.

Inhibition Evaluation on the hERG K^+ Channel. A detailed characterization is provided in the Supporting Information.

Physiochemical Properties. The physicochemical properties of the compounds were predicted using QikProp in Maestro software package. The p*K*a, LogP, and LogD values and solubility profile of compound **31** were determined experimentally by Sirius Analytical (UK) *via* UV-metric or potentiometric (pH-metric) methods (see Supporting Information for full reports).

Pharmacokinetic Assessments in SD Rats. Single-dose pharmacokinetic studies on compound **31** were performed using male Sprague-Dawley rats (n = 3 per group) in full compliance with the Guide for the Care and Use of Laboratory Animals. After intravenous injection with the compound (2 mg/kg), blood samples were collected in heparin-containing tubes at predetermined time points (0.083, 0.25, 0.5, 1, 2, 4, 8, and 24 h) and centrifuged immediately at 4 °C and 4,000 rpm for 20 min. Noncompartmental pharmacokinetic parameters were fitted using phoenix WinNonlin 6.3 based on the LC-MS/MS quantitation data.

Statistical analysis. Significance was analyzed with Student's *t* test, and the results were considered statistically significant at $p < 0.05$ (notation: *, $p < 0.05$; **, $p < 0.01$; ***, $p < 0.001$).

Molecular Modeling. Ensemble docking was performed with AutoDock4 into the predefined kinase ATP-binding pocket of PAKs. Hydrogens were added to the modelled kinase domain (PAK4 PDB code: 2X4Z; PAK1 PDB code: 4O0R), and partial atomic charges were assigned using AutoDockTools (ADT). The ligand coordinates were generated using the Corina server (www.mn-am.com/online_demos/corina_demo). The ligand was placed in the kinase ATP-binding pocket and aligned manually to avoid atom clashes. A 3D grid box (dimensions = 50×50×50 units in number of grid points; grid spacing = 0.375 Å) centered at the ATP-binding pocket was created using AutoGrid4. Docking was performed using the Lamarckian genetic algorithm in AutoDock4. Each docking experiment was performed 10 times, yielding 10 docked conformations. The solutions

were ranked by the calculated binding free energy. Figures were drawn using PyMOL.

ASSOCIATED CONTENT

Supporting Information

This material is available free of charge *via* the Internet at http://pubs.acs.org.

The sequence alignment of the active site residues of PAK1-6; the crystallographic parameters of all X-ray structures (co-crystal structures of **10a**, **30** and **31** bound to PAK4); a comparison of the orientation differences of the DFG Asp ($Asp458^{PAK4}$/$Asp407^{PAK1}$); binding mode analysis of compounds **12**, **17**, **18** and **20**; detailed kinase selectivity data of compound **31**; the ^{1}H NMR, ^{13}C NMR, and HRMS spectra of compounds **10a-d**, **11a-d**, and **12-41**; the liver microsome stability, rat plasma stability, physiochemical properties determination, CYP450 and hERG inhibition reports of compound **31** (PDF).

Molecular formula strings and associated biological data (CSV).

Accession Codes

PDB ID codes for **10a**, **30** and **31** bound to PAK4 are 5XVF, 5XVA and 5XVG, respectively.

AUTHOR INFORMATION

Corresponding Authors:

* H.L.: phone, +86 10 62771392; e-mail, lht@tsinghua.edu.cn

* F.L.: phone, +86 24 23256666; e-mail, fli@mail.cmu.edu.cn

* D.Z.: phone, +86 24 43520219; e-mail, dongmeiz-67@163.com

* M.C.: phone, +86 24 43520019; e-mail, mscheng@syphu.edu.cn

Author Contributions

[§]C.H., F.Z., H.S. contributed equally to this work.

Notes

The authors declare no competing financial interest.

ACKNOWLEDGMENTS

We thank the staff members at beamline BL17U of the Shanghai Synchrotron Radiation Facility and Dr. S. Fan at the Beijing Advanced Innovation Center for Structural Biology for their assistance in data collection. We gratefully acknowledge the financial support from the National Natural Science Foundation of China (Grant 81230077) and Program for Innovative Research Team of the Ministry of Education, and Program for Liaoning Innovative Research Team in University. H.S is grateful to the Agency for Science, Technology and Research (A*STAR), for its financial support (JCO DP Grant: 1334k00085). H.L is supported by the National Natural Science Foundation of China (Grant 31470720), and the Tsinghua University Initiative Scientific Research Program.

ABBREVIATIONS USED

ATP, adenosine triphosphate; BRAF, serine/threonine-protein kinase B-raf (raf, rapidly accelerated fibrosarcoma); CHO, Chinese hamster ovary; CL, clearance; DFG,

Asp-Phe-Gly; DSF, differential scanning fluorometry; FLT3, fms-like tyrosine kinase; hERG, human ether-a-go-go related gene; KD, kinase domain; LE, ligand efficiency; LLE, ligand lipophilicity effciency; NAMPT, nicotinamide phosphoribosyl-transferase; NSCLC, non-small cell lung cancer; PAK, p21-activated kinase; RAS, rat sarcoma; SAR, structure−activity relationship; SPR, surface plasmon resonance.

REFERENCES

1. Manser, E.; Leung, T.; Salihuddin, H.; Zhao, Z. S.; Lim, L. A brain serine/threonine protein kinase activated by Cdc42 and Rac1. *Nature* **1994,** *367*, 40-46.

2. Radu, M.; Semenova, G.; Kosoff, R.; Chernoff, J. PAK signalling during the development and progression of cancer. *Nat. Rev. Cancer* **2014,** *14*, 13-25.

3. Arias-Romero, L. E.; Chernoff, J. A tale of two Paks. *Biol. Cell* **2008,** *100*, 97-108.

4. Ye, D. Z.; Field, J. PAK signaling in cancer. *Cell. Logist.* **2012,** *2*, 105-116.

5. Senapedis, W.; Crochiere, M.; Baloglu, E.; Landesman, Y. Therapeutic potential of targeting PAK signaling. *Anticancer Agents Med.Chem.* **2016,** *16*, 75-88.

6. Rudolph, J.; Crawford, J. J.; Hoeflich, K. P.; Wang, W. Inhibitors of p21-activated kinases (PAKs). *J. Med. Chem.* **2015,** *58*, 111-129.

7. Ha, B. H.; Morse, E. M.; Turk, B. E.; Boggon, T. J. Signaling, regulation, and specificity of the type II p21-activated kinases. *J. Biol. Chem.* **2015,** *290*, 12975-12983.

8. Ha, B. H.; Davis, M. J.; Chen, C.; Lou, H. J.; Gao, J.; Zhang, R.; Krauthammer, M.; Halaban, R.; Schlessinger, J.; Turk, B. E.; Boggon, T. J. Type II p21-activated kinases (PAKs) are regulated by an autoinhibitory pseudosubstrate. *Proc. Natl. Acad. Sci. U. S. A.* **2012,** *109*, 16107-16112.

9. Kelly, M. L.; Chernoff, J. Mouse models of PAK function. *Cell. Logist.* **2012,** *2*, 84-88.

10. Tian, Y.; Lei, L.; Cammarano, M.; Nekrasova, T.; Minden, A. Essential role for the Pak4 protein kinase in extraembryonic tissue development and vessel formation. *Mech. Dev.* **2009,** *126*, 710-720.

11. Liu, Y.; Xiao, H.; Tian, Y.; Nekrasova, T.; Hao, X.; Lee, H. J.; Suh, N.; Yang, C. S.; Minden, A. The pak4 protein kinase plays a key role in cell survival and tumorigenesis in athymic mice. *Mol. Cancer Res.* **2008,** *6*, 1215-1224.

12. Callow, M. G.; Clairvoyant, F.; Zhu, S.; Schryver, B.; Whyte, D. B.; Bischoff, J. R.; Jallal, B.; Smeal, T. Requirement for PAK4 in the anchorage-independent growth of human cancer cell lines. *J. Biol. Chem.* **2002,** *277*, 550-558.

13. Minden, A. The pak4 protein kinase in breast cancer. *ISRN Oncol.* **2012,** *2012*, 694201.

14. Wells, C. M.; Jones, G. E. The emerging importance of group II PAKs. *Biochem. J.* **2010,** *425*, 465-473.

15. Rudolph, J.; Murray, L. J.; Ndubaku, C. O.; O'Brien, T.; Blackwood, E.; Wang, W.; Aliagas, I.; Gazzard, L.; Crawford, J. J.; Drobnick, J.; Lee, W.; Zhao, X.; Hoeflich, K. P.; Favor, D. A.; Dong, P.; Zhang, H.; Heise, C. E.; Oh, A.; Ong, C. C.; La, H.; Chakravarty, P.; Chan, C.; Jakubiak, D.; Epler, J.; Ramaswamy, S.; Vega, R.; Cain, G.; Diaz, D.; Zhong, Y. Chemically diverse group I p21-activated kinase (PAK) inhibitors impart acute cardiovascular toxicity with a narrow therapeutic window. *J. Med. Chem.* **2016,** *59*, 5520-5541.

16. Muller, S.; Chaikuad, A.; Gray, N. S.; Knapp, S. The ins and outs of selective kinase inhibitor development. *Nat. Chem. Biol.* **2015,** *11*, 818-821.

17. Murray, B. W.; Guo, C.; Piraino, J.; Westwick, J. K.; Zhang, C.; Lamerdin, J.; Dagostino, E.; Knighton, D.; Loi, C. M.; Zager, M.; Kraynov, E.; Popoff, I.; Christensen, J. G.; Martinez, R.; Kephart, S. E.; Marakovits, J.; Karlicek, S.; Bergqvist, S.; Smeal, T. Small-molecule p21-activated kinase inhibitor PF-3758309 is a potent inhibitor of oncogenic signaling and tumor growth. *Proc. Natl. Acad. Sci. U. S. A.* **2010,** *107*, 9446-9451.

18. Bradshaw-Pierce, E. L.; Pitts, T. M.; Tan, A. C.; McPhillips, K.; West, M.; Gustafson, D. L.; Halsey, C.; Nguyen, L.; Lee, N. V.; Kan, J. L. C.; Murray, B. W.; Eckhardt, S. G. Tumor P-glycoprotein correlates with efficacy of PF-3758309 in in vitro and in vivo models of colorectal cancer. *Front. Pharmacol.* **2013,** *4*, 22.

19. Crawford, J. J.; Lee, W.; Aliagas, I.; Mathieu, S.; Hoeflich, K. P.; Zhou, W.; Wang, W.; Rouge, L.; Murray, L.; La, H.; Liu, N.; Fan, P. W.; Cheong, J.; Heise, C. E.; Ramaswamy, S.; Mintzer, R.; Liu, Y.; Chao, Q.; Rudolph, J. Structure-guided design of group I selective p21-activated kinase inhibitors. *J. Med. Chem.* **2015,** *58*, 5121-5136.

20. Staben, S. T.; Feng, J. A.; Lyle, K.; Belvin, M.; Boggs, J.; Burch, J. D.; Chua, C. C.; Cui, H.; DiPasquale, A. G.; Friedman, L. S.; Heise, C.; Koeppen, H.; Kotey, A.; Mintzer, R.; Oh, A.; Roberts, D. A.; Rouge, L.; Rudolph, J.; Tam, C.; Wang, W.; Xiao, Y.; Young, A.; Zhang, Y.; Hoeflich, K. P. Back pocket flexibility provides group II p21-activated kinase (PAK) selectivity for type I 1/2 kinase inhibitors. *J. Med. Chem.* **2014,** *57*, 1033-1045.

21. Abu Aboud, O.; Chen, C. H.; Senapedis, W.; Baloglu, E.; Argueta, C.; Weiss, R. H. Dual and specific inhibition of NAMPT and PAK4 by KPT-9274 decreases kidney cancer growth. *Mol. Cancer Ther.* **2016,** *15*, 2119-2129.

22. Zhang, J.; Wang, J.; Guo, Q.; Wang, Y.; Zhou, Y.; Peng, H.; Cheng, M.; Zhao, D.; Li, F. LCH-7749944, a novel and potent p21-activated kinase 4 inhibitor, suppresses proliferation and invasion in human gastric cancer cells. *Cancer Lett.* **2012,** *317*, 24-32.

23. Hao, C. Z.; Huang, W. X.; Li, X. D.; Guo, J.; Chen, M.; Yan, Z. Z.; Wang, K.; Jiang, X. L.; Song, S.; Wang, J.; Zhao, D. M.; Li, F.; Cheng, M. S. Development of 2,

4-diaminoquinazoline derivatives as potent PAK4 inhibitors by the core refinement strategy. *Eur. J. Med. Chem.* **2017,** *131*, 1-13.

24. Hao, C. Z.; Li, X. D.; Song, S.; Guo, B. Y.; Guo, J.; Zhang, J.; Zhang, Q. L.; Huang, W. X.; Wang, J.; Lin, B.; Cheng, M. S.; Li, F.; Zhao, D. M. Advances in the 1-phenanthryl-tetrahydroisoquinoline series of PAK4 inhibitors: potent agents restrain tumor cell growth and invasion. *Org. Biomol. Chem.* **2016,** *14*, 7676-7690.

25.Senisterra, G.; Chau, I.; Vedadi, M. Thermal denaturation assays in chemical biology. *Assay. Drug. Dev. Technol.* **2012,** *10*, 128-136.

26. Homola, J. Surface plasmon resonance sensors for detection of chemical and biological species. *Chem. Rev.* **2008,** *108*, 462-493.

27. Pierce, A. C.; Sandretto, K. L.; Bemis, G. W. Kinase inhibitors and the case for CH...O hydrogen bonds in protein-ligand binding. *Proteins* **2002,** *49*, 567-576.

28. Hopkins, A. L.; Groom, C. R.; Alex, A. Ligand efficiency: a useful metric for lead selection. *Drug. Discov. Today.* **2004,** *9*, 430-431.

29. Leeson, P. D.; Springthorpe, B. The influence of drug-like concepts on decision-making in medicinal chemistry. *Nat. Rev. Drug. Discov.* **2007,** *6*, 881-890.

30. Eswaran, J.; Lee, W. H.; Debreczeni, J. E.; Filippakopoulos, P.; Turnbull, A.; Fedorov, O.; Deacon, S. W.; Peterson, J. R.; Knapp, S. Crystal Structures of the p21-activated kinases PAK4, PAK5, and PAK6 reveal catalytic domain plasticity of active group II PAKs. *Structure* **2007,** *15*, 201-213.

31.van Linden, O. P.; Kooistra, A. J.; Leurs, R.; de Esch, I. J.; de Graaf, C. KLIFS: a knowledge-based structural database to navigate kinase-ligand interaction space. *J. Med. Chem.* **2014,** *57*, 249-277.

32. Kooistra, A. J.; Kanev, G. K.; van Linden, O. P.; Leurs, R.; de Esch, I. J.; de Graaf, C. KLIFS: a structural kinase-ligand interaction database. *Nucleic. Acids. Res.* **2016,** *44*, D365-371.

33. Vulpetti, A.; Bosotti, R. Sequence and structural analysis of kinase ATP pocket residues. *Farmaco* **2004,** *59*, 759-765.

34. Ruegg, U. T.; Burgess, G. M. Staurosporine, K-252 and UCN-01: potent but nonspecific inhibitors of protein kinases. *Trends. Pharmacol. Sci.* **1989,** *10*, 218-220.

35. Gilli, G. G. a. P. *The Nature of the Hydrogen Bond*. Oxford University Press Inc.: New York, 2009.

36. Wang, R. X.; Lai, L. H.; Wang, S. M. Further development and validation of empirical scoring functions for structure-based binding affinity prediction. *J. Comput. Aid. Mol. Des.* **2002,** *16*, 11-26.

37. Wolber, G.; Langer, T. LigandScout: 3-d pharmacophores derived from protein-bound Ligands and their use as virtual screening filters. *J. Chem. Inf. Model.* **2005,** *45*, 160-169.

38. Cai, S.; Ye, Z.; Wang, X.; Pan, Y.; Weng, Y.; Lao, S.; Wei, H.; Li, L. Overexpression of P21-activated kinase 4 is associated with poor prognosis in

non-small cell lung cancer and promotes migration and invasion. *J. Exp. Clin. Canc. Res.* **2015,** *34*, 48.

39. Mitcheson, J. S. hERG potassium channels and the structural basis of drug-induced arrhythmias. *Chem. Res. Toxicol.* **2008,** *21*, 1005-1010.

40. Su, Q. B.; Ioannidis, S.; Chuaqui, C.; Almeida, L.; Alimzhanov, M.; Bebernitz, G.; Bell, K.; Block, M.; Howard, T.; Huang, S.; Huszar, D.; Read, J. A.; Costa, C. R.; Shi, J.; Su, M.; Ye, M. W.; Zinda, M. Discovery of 1-methyl-1*H*-imidazole derivatives as potent Jak2 inhibitors. *J. Med. Chem.* **2014,** *57*, 144-158.

41. Sakamoto, T.; Moriya, M.; Tsuge, H.; Takahashi, T.; Haga, Y.; Nonoshita, K.; Okamoto, O.; Takahashi, H.; Sakuraba, A.; Hirohashi, T.; Shibata, T.; Kanno, T.; Ito, J.; Iwaasa, H.; Gomori, A.; Ishihara, A.; Fukuroda, T.; Kanatani, A.; Fukami, T. Novel orally active NPY Y5 receptor antagonists: synthesis and structure-activity relationship of spiroindoline class compounds. *Bioorg. Med. Chem.* **2009,** *17*, 5015-5026.

42. Adams, P. D.; Afonine, P. V.; Bunkoczi, G.; Chen, V. B.; Davis, I. W.; Echols, N.; Headd, J. J.; Hung, L. W.; Kapral, G. J.; Grosse-Kunstleve, R. W.; McCoy, A. J.; Moriarty, N. W.; Oeffner, R.; Read, R. J.; Richardson, D. C.; Richardson, J. S.; Terwilliger, T. C.; Zwart, P. H. PHENIX: a comprehensive Python-based system for macromolecular structure solution. *Acta Crystallogr. D.* **2010,** *66*, 213-221.

43. Emsley, P.; Lohkamp, B.; Scott, W. G.; Cowtan, K. Features and development of Coot. *Acta Crystallogr. D.* **2010,** *66*, 486-501.

44. Cheng, Y.; Prusoff, W. H. Relationship between the inhibition constant (Ki) and the concentration of inhibitor which causes 50 per cent inhibition (IC_{50}) of an enzymatic reaction. *Biochem. Pharmacol.* **1973,** *22*, 3099-3108.

45. Song, H. Y.; Smith, R. A. A.; Hao, C. Z.; Wang, J.; Dahlroth, S. K. S.; Cheng, M. S.; Fernig, D. G.; Gorelik, S.; Nurcombe, V. *Unpublished results.*

46. Ma, Y.; Sun, G.; Chen, D.; Peng, X.; Chen, Y. L.; Su, Y.; Ji, Y.; Liang, J.; Wang, X.; Chen, L.; Ding, J.; Xiong, B.; Ai, J.; Geng, M.; Shen, J. Design and optimization of a series of 1-sulfonylpyrazolo[4,3-b]pyridines as selective c-Met inhibitors. *J. Med. Chem.* **2015,** *58*, 2513-2529.

Table of contents graphic

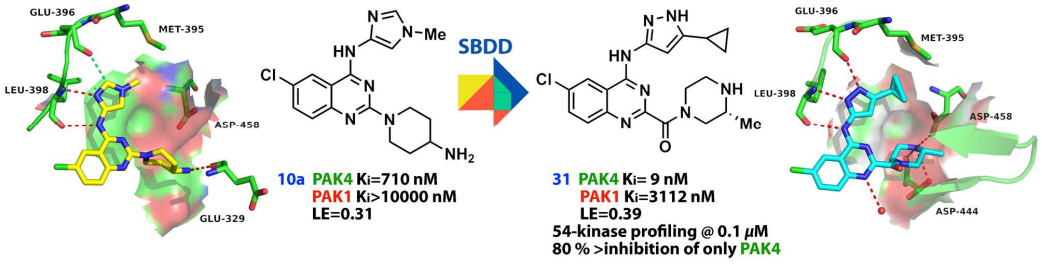

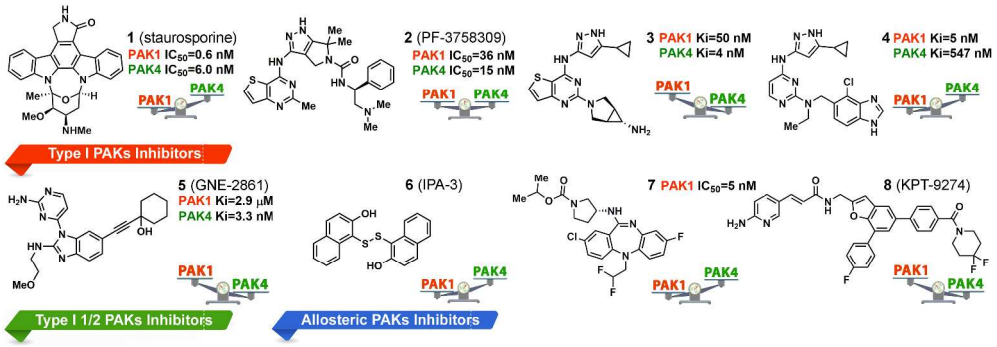

Figure 1. Classification of representative PAK inhibitors by mechanism of function.

338x116mm (300 x 300 DPI)

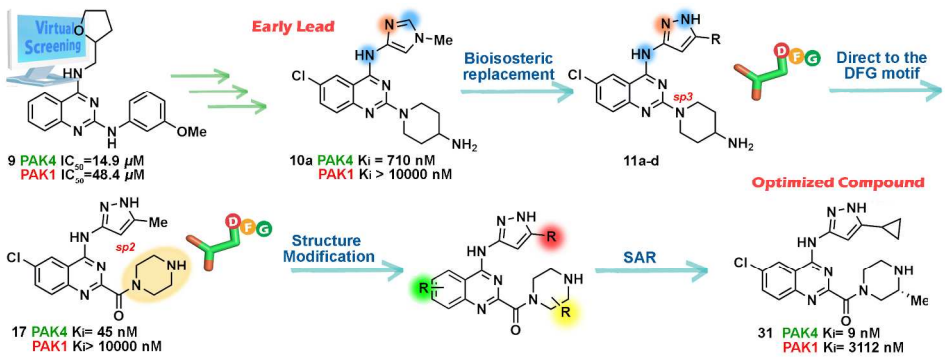

Figure 2. The design and modification strategies of novel and selective PAK4 inhibitors.

226x80mm (300 x 300 DPI)

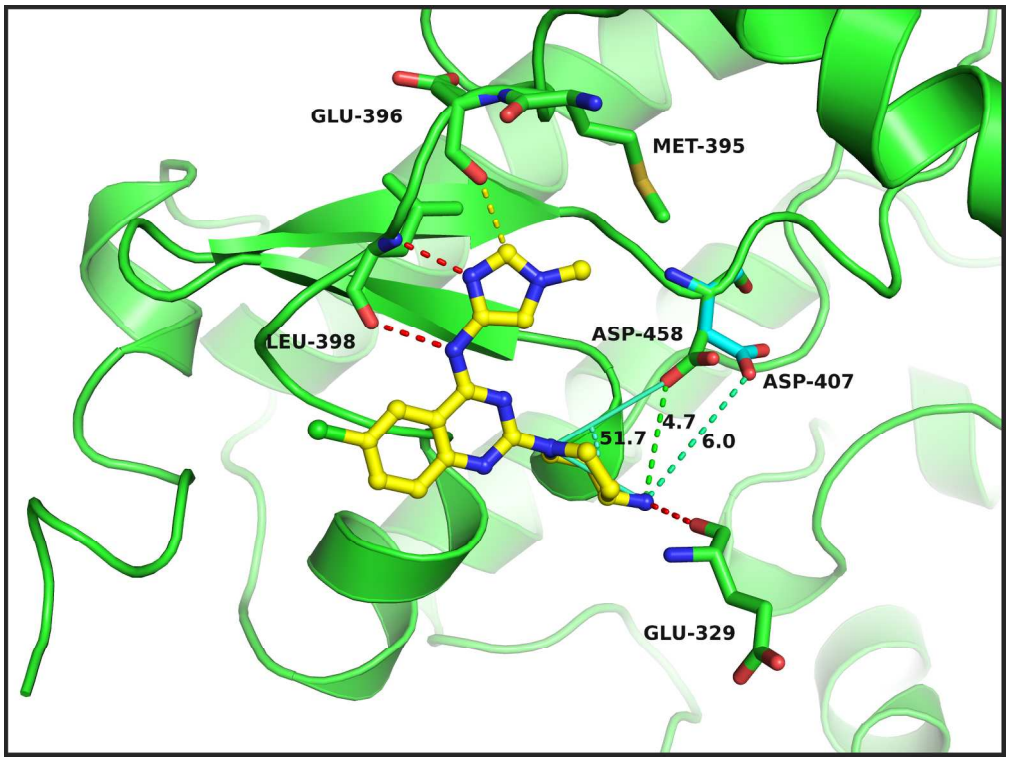

Figure 3. The crystal structure of PAK4 in complex with 10a (PDB code 5XVF). Note: Asp458 is oriented towards the NH2 in the piperidine of 10a compared to its counterpart Asp407 in PAK1 as in the structure 4O0R (cyan stick). The distance between the piperidine NH2 of 10a and the carboxyl group (OD2 atom) of Asp458PAK4 and Asp407PAK1 is 4.7 Å and 6.0 Å, respectively (green line). The ∠O(Asp458)−N(piperidine N)−N(piperidine NH2) angle is approximately 51.7° (cyan line).

203x152mm (300 x 300 DPI)

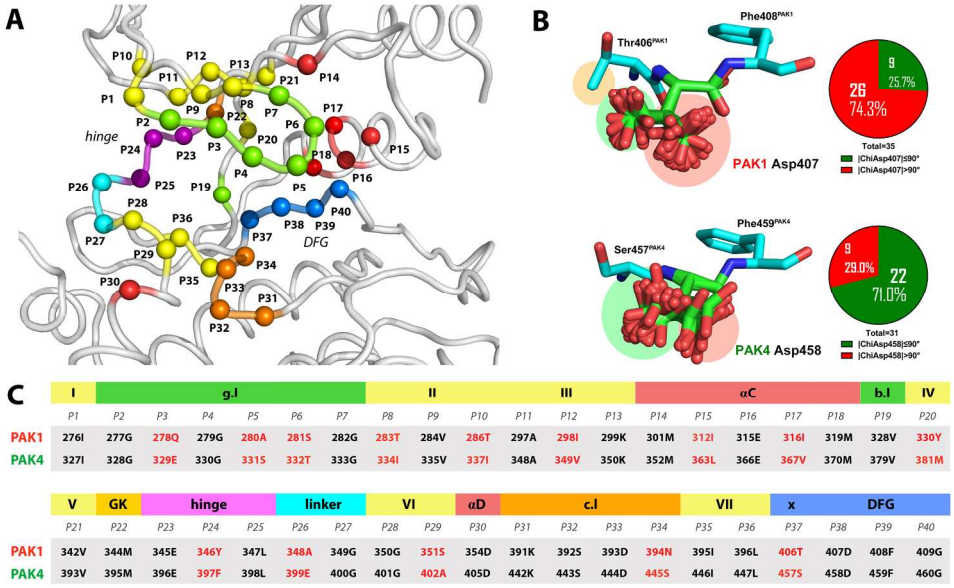

Figure 4. A comparison of the ATP-binding pocket between group I and II PAKs. (A) The structure of the PAK kinase domain (generated from the PDB structure 2X4Z). Residues contributing to the binding cleft (P1-P40) are depicted as spheres. (B) Alignment (main chain atoms only) of the DFG-aspartate of PAK1 and PAK4 in the active state. An updated survey of all PDB PAK1 structures in the active DFG-in state indicated that 74 % (26/35) of the DFG-aspartate side chain is pointing away from the ATP-competitive ligand. For the corresponding residue in PAK4, 71 % (22/31) of the DFG-aspartate side chain is pointing toward the ligand. Figures were generated using PyMOL (The PyMOL Molecular Graphics System, Version 1.7.2 Schrödinger, LLC.). The definition of the dihedral angles χ1(chi): N-Cα-Cβ-Cγ. (C) Sequence alignment of the residues surrounding the ATP binding site in PAK1 and PAK4. Differential residues between the two kinases are highlighted.

211x130mm (300 x 300 DPI)

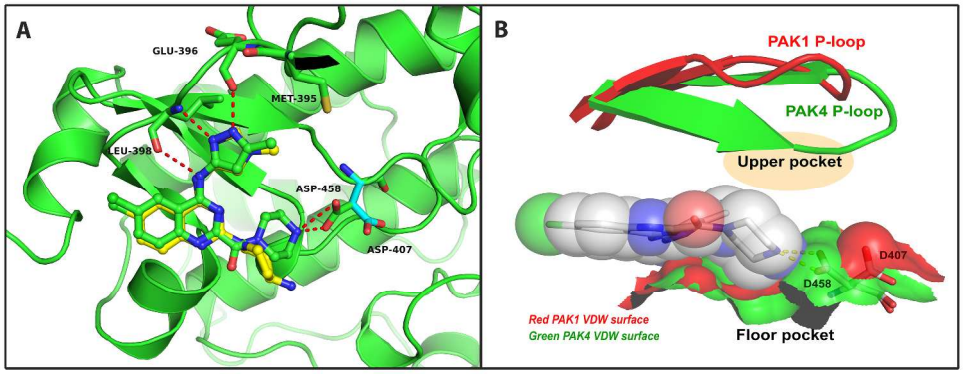

Figure 5. The predicted binding mode of 17. (A) The superimposition of structures of 17 (green) with 10a from the crystal structure (PDB code 5XVF). PDB entry 2X4Z was used for molecular docking simulation with Autodock4. Note: Asp458 in PAK4 overlaid with a key residue different in PAK1 (cyan, Asp407 from structure 4O0R). (B) The overlay of PAK4 and PAK1 with 17 (generated from the PDB structures 2X4Z and 4O0R, respectively).

406x169mm (300 x 300 DPI)

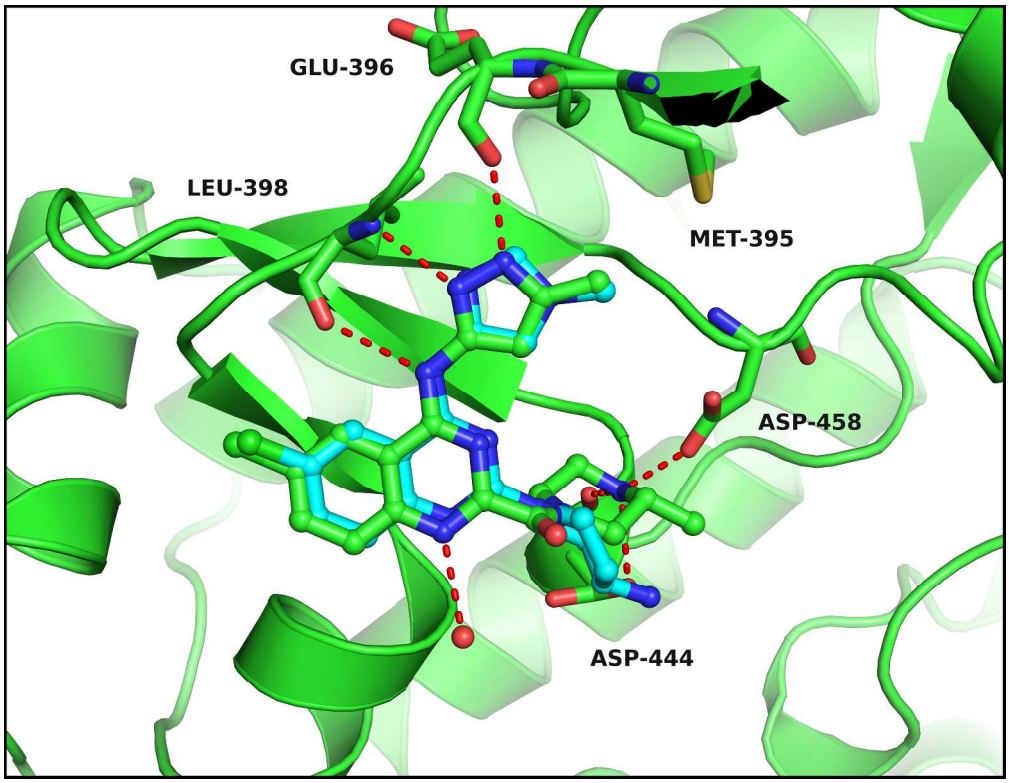

Figure 6. The crystal structure of PAK4 in complex with 30 (PDB code 5XVA). The superimposition of the structures of 30 (green) with 10a (cyan) from the crystal structure (PDB code 5XVF).

307x237mm (300 x 300 DPI)

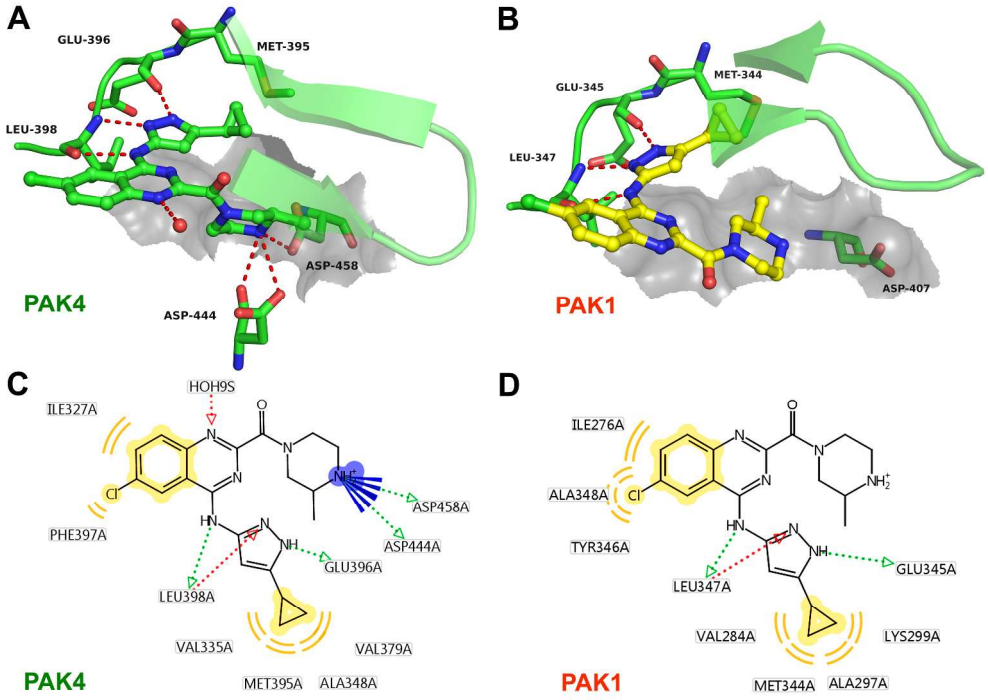

Figure 7. (A) The crystal structure of PAK4 in complex with 31 (PDB code 5XVG). (B) The predicted binding mode of 31 in PAK1 (PDB code 4O0R). A schematic representation of the contacts between 31 and the binding site residues of PAK4 (C) and PAK1 (D) was visualized by LigandScout. Note: the piperazine ring of 31 provides charge-assisted hydrogen bond (CAHB) interactions with Asp458PAK4 and Asp444PAK4.

265x189mm (300 x 300 DPI)

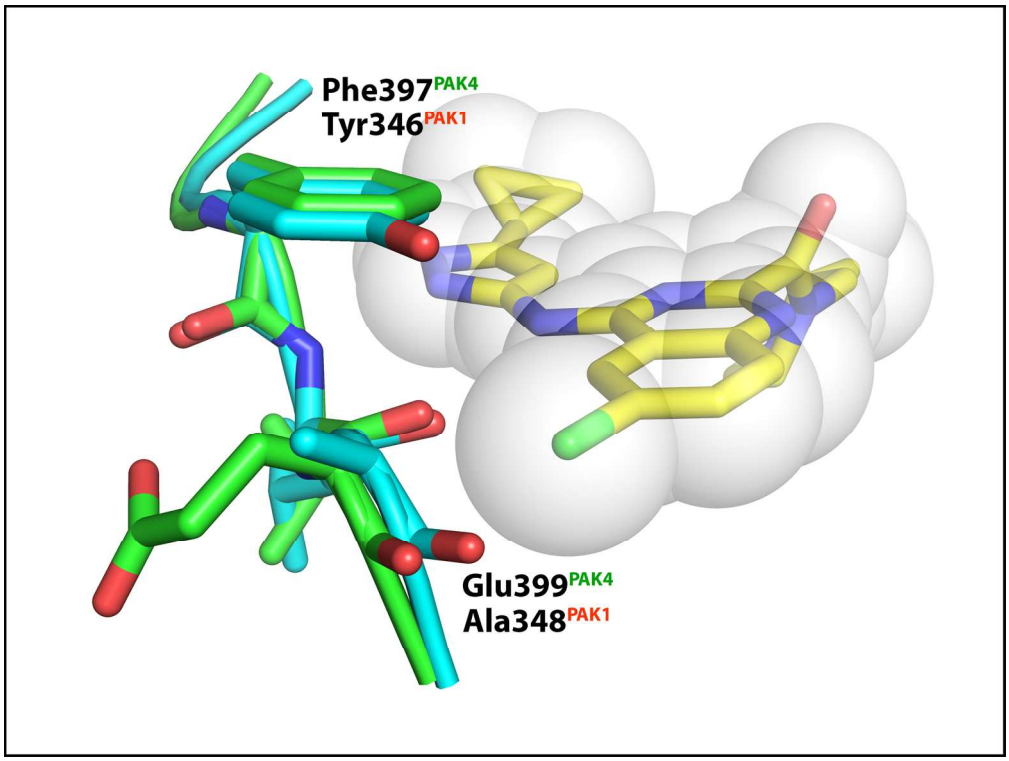

Figure 8. The microenvironment of the 6-substituent of the inhibitors. The X-ray structure of 31 in complex with PAK4 (green, PDB 5XVG) overlaid with key residue differences with PAK1 (cyan, Tyr346 and Ala348 from structure 4O0R).

169x127mm (300 x 300 DPI)

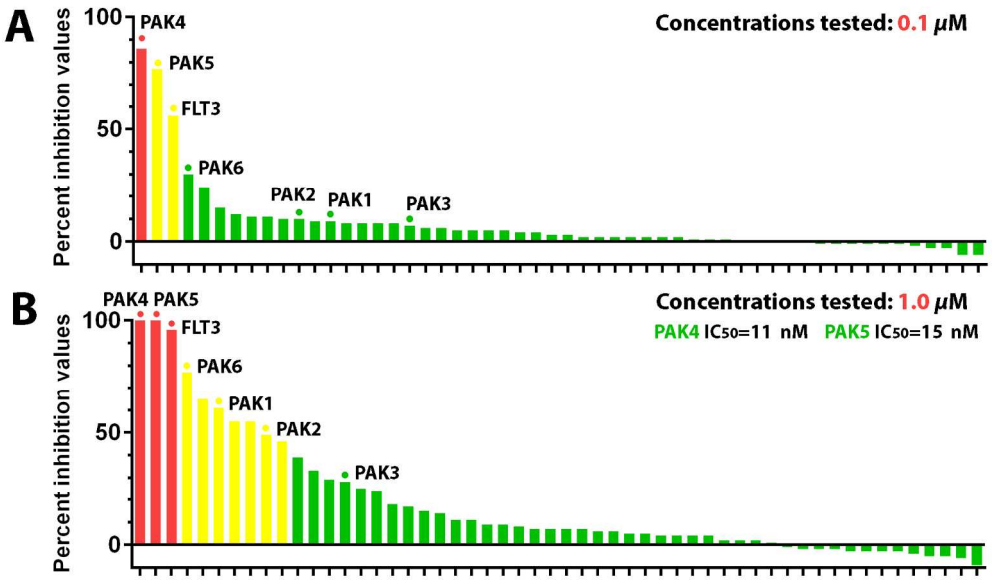

Figure 9. Selectivity profile of compound 31 (A) measured at a concentration of 0.1 μM and (B) 1.0 μM in a panel of 54 kinases generated with the SelectScreen® Profiling Service from Life Technologies (red columns denote >80 %, yellow columns between 40 and 80 %, and green columns <40 % inhibition).

179x108mm (300 x 300 DPI)

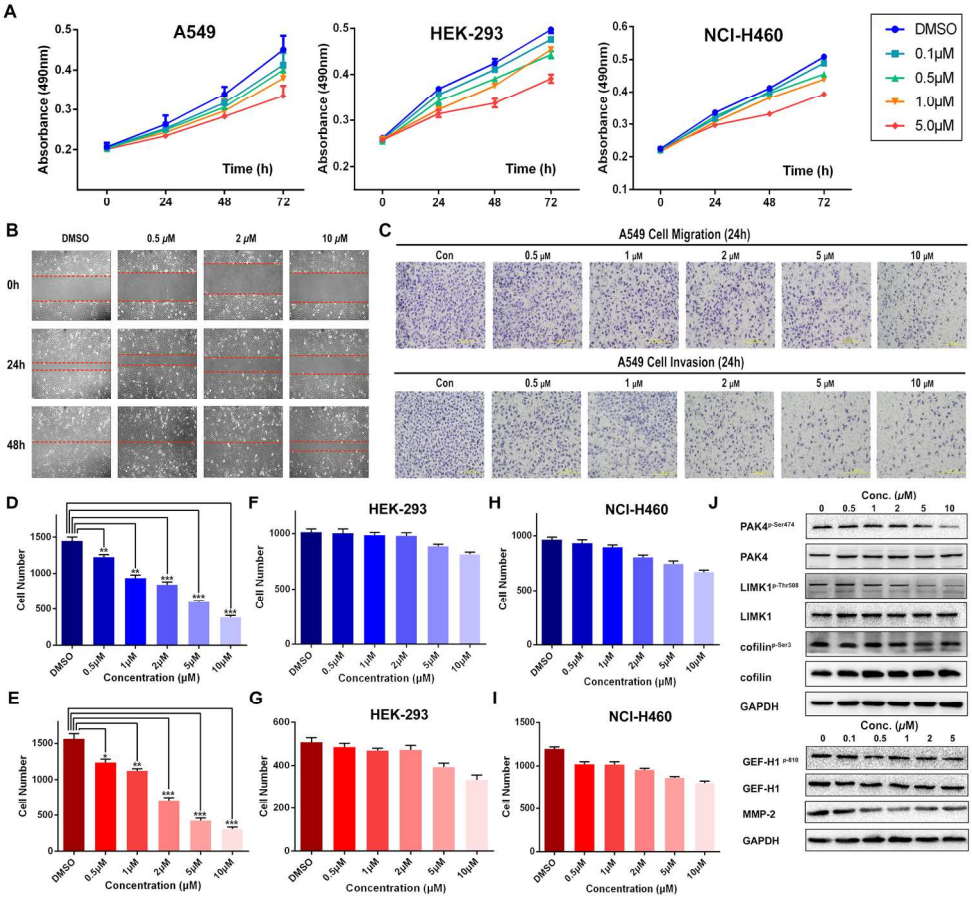

Figure 10. Compound 31 suppresses the migratory and invasive potential of A549 lung cancer cells via inhibition of PAK4 kinase activity and its downstream pathways. (A) MTT assay showed the anti-proliferative effect of compound 31 on A549, HEK-293 and NCI-H460 cells. (B) Compound 31 inhibits migration of A549 lung cancer cells in a wound healing assay. (C-F) Transwell assay [-(D)/+ (C) matrigel] was performed to show the effect of indicated concentrations of 31 on A549 lung cancer cells migration (C) and invasion (D). And migrated cells were counted respectively (E-F). The results are presented as the mean ± standard deviation (*, $p < 0.05$; **, $p < 0.01$; ***, $p < 0.001$ vs control). (G-H) Effect of 31 on HEK-293 cells migration (G) and invasion (H). (I-J) Effect of 31 on NCI-H460 cells migration (I) and invasion (J). Scale bar, 500 μm. (K) Western blot assay showed the effect of compound 31 on the phospho-PAK4 Ser474 level and on the phosphorylation levels of PAK4 downstream targets LIMK1 and cofilin. The expression of MMP-2 and the phosphorylation of GEF-H1 were also downregulated by compound 31 treatment in a dose-dependent manner. A549 cells were cultured with vehicle or the indicated concentrations of compound 31 for 24 h, and then proteins were extracted and subjected to analysis.

173x157mm (300 x 300 DPI)

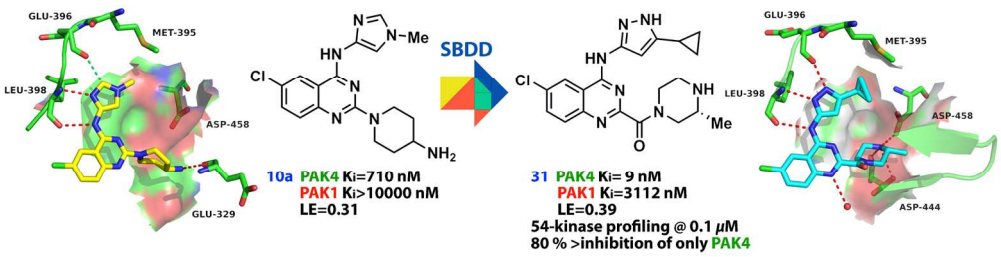

Table of contents graphic

170x47mm (300 x 300 DPI)